The Journal of Undergraduate Research in Physics

CONTENTS

ON PREPARING A MANUSCRIPT FOR PUBLICATION.....1
Rexford E. Adelberger, Editor

NONLINEAR OPTICAL ABSORPTION IN ZnSe.....5
John G. Bognar
Wright State University

DETERMINATION OF THE TEMPERATURE DEPENDENCE OF THE BAND GAP ENERGY OF A GaAs LED FROM MEASUREMENTS OF ITS EMISSION SPECTRA.....11
Zhen-Hong Zhou
Polytechnic University

UNUSUAL PROCESSES IN THE ELECTRON IMPACT IONIZATION OF 1,2 DICHLORO-ETHANE.....19
Zoran Psenicnik
Syracuse University

THE MADELUNG ENERGY OF THE SUPERCONDUCTOR $YBa_2Cu_3O_7$.....25
Kenneth A. Ritley
Oak Ridge National Laboratory

MEASUREMENT OF COAGULATION PROCESSES BY LIGHT SCATTERING TECHNIQUES.....33
Lee Fraiji
Union College

Post Use Book Review -.....37
Physics for Scientists and Engineers, 2nd. Ed.
R.A. Serway
Reviewed by Jodi L. Barnhill
University of Arizona

VOLUME 8, NUMBER 1

OCTOBER 1989

Published by the Physics Department of Guilford College
for
The American Institute of Physics and The Society of Physics Students

THE JOURNAL OF UNDERGRADUATE RESEARCH IN PHYSICS

This journal is devoted to research work done by undergraduate students in physics and its related fields. It is to be a vehicle for the exchange of ideas and information by undergraduate students. Information for students wishing to submit manuscripts for possible inclusion in the Journal follows.

ELIGIBILITY

The author must have performed all work reported in the paper as an undergraduate. The subject matter of the paper is open to any area of pure or applied physics or physics related field.

SPONSORSHIP

Each paper must be sponsored by a full-time faculty member of the department in which the research was done. A letter from the sponsor, certifying that the work was done by the author as an undergraduate and the the sponsor is willing to be acknowledged in the paper, must accompany the manuscript if it is to be considered for publication.

SUBMISSION

Two copies of the manuscript, the letter from the sponsor and a telephone number where the author can be reached should be sent to:

Dr. Rexford E. Adelberger, Editor
THE JOURNAL OF UNDERGRADUATE
RESEARCH IN PHYSICS
Physics Department
Guilford College
Greensboro, NC 27410

FORM

The manuscript should be typed, double spaced, on 8 1/2 x 11 inch sheets. Margins of about 1.5 inches should be left on the top, sides, and bottom of each page. Papers should be limited to fifteen pages of text in addition to an abstract (not to exceed 250 words) and appropriate drawings, pictures, and tables. Manuscripts may be submitted on a disk that can be read by a MacIntosh™. The files must be compatible with MacWrite™ or MicroSoft Word™. Illustrations should be in a MacDraw™ or MacPaint™ PICT format.

ILLUSTRATIONS

Line drawings should be made with black ink on plain white paper. Each figure or table must be on a separate sheet. Photographs must have a high gloss finish.

CAPTIONS

A brief caption should be provided for each illustration or table, but it should not be part of the figure. The captions should be listed together at the end of the manuscript

EQUATIONS

Equations should appear on separate lines, and may be written in black ink.

FOOTNOTES

Footnotes should be typed, double spaced and grouped together in sequence at the end of the manuscript.

SUBSCRIPTION INFORMATION

The Journal is published bianually, with issue one appearing in October and issue two in April of the next year. There are two issues per volume.

TYPE OF SUBSCRIBER	PRICE PER VOLUME
Individual	$US 5.00
Institution	$US 10.00

Foreign subscribers add $US 2.00 for surface postage, $US 10.00 for air freight.

To receive a subscription, send your name, address, and check made out to **The Journal of Undergraduate Research in Physics (JURP)** to the editorial office:

JURP
Physics Department
Guilford College
Greensboro, NC 27410

Back issues may be purchased by sending $US 15.00 per volume to the editorial office.

The *Journal of Undergraduate Research in Physics* is published by the Physics Department of Guilford College for the American Institute of Physics and the Society of Physics. **ISSN 0731-3764**

VOLUME 8 1989-90

The Journal of Undergraduate Research in Physics

Published by the Physics Department
of Guilford College
for

The American Insitute of Physics
and
The Society of Physics Students

ISSN 0731 - 3764

ON PREPARING A MANUSCRIPT FOR PUBLICATION

Rexford E. Adelberger, Editor

Perhaps the most important thing for you to keep in mind when you write a manuscript which you intend to submit for publication to the Journal of Undergraduate Research in Physics is who the audience is that will be reading the paper. The majority of the readers of the Journal are junior or senior physics majors. They are knowledgeable about physics, but unlike you, they have not spent as much time trying to understand the specific work which is being reported in your paper. They also can read English well and expect the paper to be written by a colleague, not a robot or an 'all-knowing' computer. There is a big difference between the comments you write in the margin of your lab notebook or what you might write in a technical brief and what you should present in a paper for publication in a scientific journal.

The general style of writing that should followed when preparing a manuscript for publication in the Journal is different from what you would submit to your English literature professor as a critique of some other work. The narrative is intended to do three things:

1) set the background necessary so that the reader can appreciate and understand the physics being reported;
2) discuss the details of what you did and the implications of your work;
3) lead the reader through the work in such a way that they must come to the same concluding points that you did.

When the readers finish with your paper, they should not have to go back and try to decide for themselves what you did. Your narrative should lead them through your work in an unambiguous manner, telling them what to see and understand in what you did. The interpretation of the data or calculations should be done by the writer, not the reader.

You should take care to make sure that the material is presented in a concise logical way. You should make sure that your sentences do not have too many dependent clauses. Overly complicated sentences make the logic of an argument difficult to follow. You should choose a paragraph structure which focuses the attention of the reader on the development of the ideas.

A format which often achieves these aims is suggested below:

ABSTRACT

An abstract is a self contained paragraph that concisely explains what you did and presents any interesting results you found. The abstract is often published separately from the body of the paper, so you cannot assume that the reader of the abstract also has a copy of the rest of the paper. Abstracts are used in computerized literature searches, so all key words that describe the paper should be included in it.

INTRODUCTION

This is the section that sets the background for the important part of the paper. It is not just an abbreviated review of what you are going to discuss in detail later. This narrative should present the necessary theoretical and experimental background such that a knowledgeable colleague, who might not be expert in the field, will be able to understand the data presentation. If you are going to use a particular theoretical model to extract some formation from your data, this model should be discussed in the in-

troduction.

Where appropriate, the information should be referenced. When presenting background information, you can guide the reader to a detailed description of a particular item with the statement such as: "*Amore detailed discussion of laminar flow can be found elsewhere*[1]". If you know where there is a good discussion of some item, you don't have to repeat it, just guide the reader to the piece.

How one proceeds from this point depends upon whether the paper is about a theoretical study or is a report on an experiment. I will first suggest a format for papers about experimental investigations and then one that describes a theoretical derivation.

Papers about experimental investigations

THE EXPERIMENT

This section guides the reader through the techniques and apparatus used to generate the data. Schematic diagrams of equipment and circuits are often easier to understand than prose descriptions. A statement such as "*A diagram of the circuit used to measure the stopping potential is shown in Figure 6*" is better than a long elegant set of words. It is not necessary to describe in words what is shown in a diagram unless you feel that there is a very special part which should be pointed out to the reader. If special experimental techniques were developed as part of this work, they should be discussed here.

DATA PRESENTATION

This is the most important section of the paper. The data (a plural noun) are the truths of your work. This section should lead the reader through the data and how errors were assigned. The numerical data values are presented in tables and graphs, each with its own caption. All figures should be referred to by their number.

Any graph or table that is not discussed in the narrative should be eliminated. Items which are not discussed have no place in a paper. A well written data presentation results in a reader who reaches the same conclusion as the author about the experiment.

A paper which reports on a theoretical study should include the following sections:

THE MODEL

This part should consist of a theoretical development of the constructs used to model the physical system under investigation. Formulae should be on separate lines and numbered consecutively. The letters or symbols used in the equations should be identified in the narrative. An example is shown below.

The potential can be approximated as:

$$W \approx Z - \sigma(\rho) \qquad (1)$$

where Z is the number of protons and σ is the screening constant that is dependent on the charge density ρ of the inner electrons of the K and L shells.

You should be sure to distinguish between what is your work and that of others by using end-notes. You should eliminate phrases such as: "*one can easily show that...*". You should not try to intimidate the reader. Remember that the reader of your paper is a senior in college!

CALCULATIONS

This section presents a summary and discussion of the numerical results calculated from the model. These results should be presented in tables or graphs, each with their own caption. A table or graph which is not discussed in the narrative should be eliminated. Data that are not interpreted by the writer have no place in a paper. One should take care to reference numerical results, if they come from someone else, which are used in the calculations.

The following sections and comments pertain to both types of papers.

CONCLUSIONS

It is indeed rare that one can come to clear and meaningful conclusions in one paper. I do not know of many papers where this section should be included. What you might do is include a summary of your work.

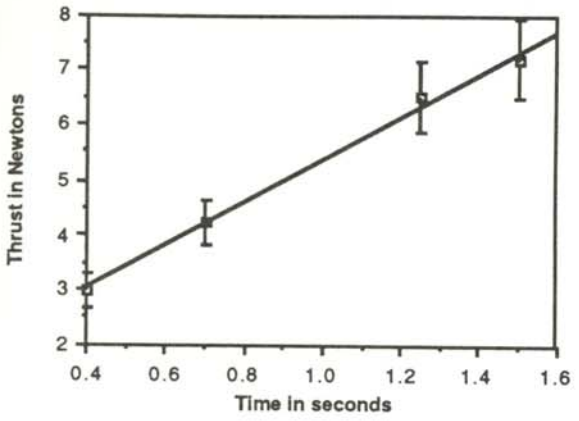

Figure 1
A graph of the measured trust of a D-2 engine as a fuction of time. The line drawn is the least sqauares fit straight line to the data.

SUMMARY

This section would include a review of all important results. Comparisons (in terms of standard deviations) of your results with those found elsewhere should be done here. This section might also include suggestions for further research that could be done on this topic.

REFERENCES

All references, numbered in order from beginning to end of the paper, are collected together at the end of the paper. You should be aware of the following format:

If the reference is a text-

1) A.J. Smith and Q.C.S. Smythe, Electromagnetic Theory, Addison Wesley, New York, 1962, p. 168.

If the reference is a journal-

2) J. Botswain, Journal of Important Results, 92, 1968, pp. 122-127.

If the reference is unpublished-

3) R.J. Ralson, private communication.

ACKNOWLEDGMENTS

This short section should acknowledge the help received (that is not referenced in the previous section) from others. This is where you would give credit to a lab partner or someone in the machine shop who helped you build a piece of equipment. *The following is a set of suggestions that will make your paper easier to understand.*

Figures or Tables

Tables and figures are placed at the corners of the page. It might happen that a figure is not on the same page as the discussion of the figure. Consequently, each table or figure should be numbered and have a caption which explains the figure. An example of a graph of a set of data is shown in Figure 1. You should notice that the graph fits the enclosed box, error bars are shown with the data points and all lines drawn on the graph are identified. A figure or table that is not discussed in the narrative part of the report serves no purpose and should eliminated.

You should be careful that the figures you present are not too busy. If you try to put too much information on a single figure, it becomes difficult for the reader to pick out the important parts. The object of the paper is to bring the reader to an understanding of what you did rather than to direct a game of hide-and-seek.

Any experimentally measured numbers used in tables should include an uncertainty. You should use scientific notation when presenting numbers, e.g. $(7.34 \pm .03) \times 10^7$ eV. You should take care to have the correct number of significant digits in your results. Just because the computer prints out 6 digits does not mean that they are significant. You should use the MKS system of units.

A few comments on style

It is often helpful to make a flow chart of your paper before you write it. In this way, you can be sure that the logical development of your presentation does not resemble two octopuses fighting, but is linear.

You should stay away from clauses such as: *'It is easy to see'* or *'one clearly sees'*. Such statements only intimidate the reader that does not find your work trivial.

It is often confusing when you begin sentences with conjunctions. Make sure that each sentence is a clear positive statement rather than an apology.

NONLINEAR OPTICAL ABSORPTION IN ZnSe

John G. Bognar
Department of Physics
Wright State University
Dayton, OH 45435

ABSTRACT

The two-photon absorption coefficient of zinc selenide was determined by measuring the input and output intensities as a laser pulse passed through a sample of ZnSe. Measurements were made at room temperature and at 10 K using 12 ns and 35 ps Nd:YAG laser pulses of 0.532 μm wavelength. Neutral density filters were used to vary intensity between 2MW/cm^2 and 0.3GW/cm^2 using nanosecond pulses, and between 200MW/cm^2 and 22GW/cm^2 using picosecond pulses, through a 2 mm thick sample with no damage occurring. A high speed streak-camera and a pyroelectric joulemeter were used to obtain the data required to calculate input and output intensities from which the absorption coefficient was obtained.

INTRODUCTION

The nonlinear absorptive properties of certain semiconductor materials make them possible candidates for use in optical limiting devices. Such devices, which have high transmission at low input intensities and low transmission at high input intensities, have been demonstrated[1] to have picosecond turn on time. These devices can be used as protective elements to restrict the high intensities of light incident upon sensitive optical components or as regulators to smooth high optical transients, as a Zener diode does in electrical systems. Moreover, the extremely fast switching times make these devices attractive for use in optical computers. The combining of optical nonlinearities with feedback has been shown[2] to produce optical bistability which can be used to develop optical logic gates. The number of possible uses of nonlinear optical materials makes an investigation of their properties a worthwhile venture.

Nonlinear absorption in samples of single crystal ZnSe, a group II-VI semiconductor compound, was investigated. Specifically, the two photon absorption coefficient of ZnSe was determined. The effects of other nonlinear phenomena were considered, and experimental parameters were varied in order to weigh their effects.

TWO PHOTON ABSORPTION

When a photon is incident upon an atom, an electron in the atom may make a transition to a higher excited state if the photon energy (hν) is greater than the energy difference between allowed states. If the photon energy is not greater than the first en-

---

John graduated from Wright State University this year. Some of this work was done at Wright Patterson Air Force Base. This is the second paper that John has had published in the Journal.

ergy difference or bandgap, Eg, no transition will occur. However, if two photons appear simultaneously at the same location in the atom, their energies can combine (by summation) to an energy greater than Eg, thereby causing a transition. This event is two photon absorption (2PA). Since a high density of photons is required for a probability of two to appear together, the probability of 2PA occurring is greater at high intensities (MW/cm^2 - GW/cm^2)[1]. Since the probability of 2PA is related to the square of the number of photons divided by the number of states, it is a nonlinear phenomenon.

The bandgap of ZnSe ranges from 2.8 eV at 0 K to 2.67 eV at 300 K. This range exists because an increase in temperature causes an increase in the lattice phonon population which increases electron-phonon interaction resulting in reduced electron energies and a lower conduction band [3]. The energy of a photon of wavelength 0.532 μm is:

$$\begin{aligned} E &= h\upsilon \\ &= (4.14 \times 10^{-15}\ \text{eV s})(5.63 \times 10^{14}\ \text{Hz}) \\ &= 2.33\ \text{eV} \end{aligned} \quad (1)$$

Therefore, a single photon of this wavelength has insufficient energy to cause an electronic transition, whereas two photon absorption is energetically possible.

An alternative to describing an electron's gain of energy in an absorption process is to describe the loss of energy in a pulse of light as it travels through the absorbing medium. The modeling of this loss process leads to expressions for the desired absorption coefficients of the medium. This loss can be described by the differential equation:

$$\frac{dI}{dx} = -\alpha I - \beta I^2 \quad (2)$$

where I is the light intensity a distance x into the absorbing medium. The loss scales linearly in the first term, where α is the linear absorption coefficient, and quadratically with the second term where β is the nonlinear absorption coefficient. The solution to this equation where losses due to reflection are also considered, in its usable form, is:

$$\frac{I_{in}}{I_{out}} = \frac{\beta(e^{\alpha L} - 1)}{\alpha(1 - R)} I_{in} + \frac{e^{\alpha L}}{(1 - R)^2} \quad (3)$$

where L is the sample thickness and R is the reflection at the front surface of the medium (the rear surface reflection which can be significant in high index materials[1] is ignored.) This solution has the equation of a straight line, where I_{in} is the independent variable. The absorption coefficients can be solved from the expressions for the slope and the y-intercept of the I_{in}/I_{out} vs I_{in} line:

$$\alpha = \frac{\ln[b(1-R)^2]}{L} \quad (4)$$

$$\beta = \frac{m\alpha(1 - R)}{e^{\alpha L} - 1} \quad (5)$$

where m is the slope and b is the y-intercept. Determinations of output intensity versus input intensity and a subsequent plot of I_{in}/I_{out} vs I_{in} were made, where the incident intensity was assumed to have constant temporal and spatial Gaussian profiles. The coefficients were then calculated from the slope and intercept of the resulting line.

Pulse intensities (or fluences) were determined by measuring pulse energies (E in joules), temporal full-width-half-max (FWHM) pulse widths (t in sec), and FWHM pulse diameters (d in cm). These measurements were combined to obtain intensities by the equation:

$$I = \frac{E}{t\left(\frac{d}{2}\right)^2 \pi} \quad (6)$$

The nonlinear coefficient that is determined results from the combination of all nonlinearly absorbing phenomena. Forms of nonlinear absorption other than 2PA include two-step absorption and absorption due to the generation of free carriers. In two-step absorption a single photon may cause an electron to make a transition to an intermediate state with a finite lifetime, followed by a second photon which causes a transition from the intermediate state to the conduction band. The probability of

two-step absorption occurring is related to the lifetime of the intermediate state which may be longer or shorter than the pulse length.

To examine the effect of pulse length on the absorption coefficient, pulses of FWHM temporal lengths of 12 ns and 35 ps were used. Free carrier generation in a semiconductor[4] is a temperature dependent phenomenon[5]. To examine how this would affect results, intensity measurements were made at room temperature and at 10 K.

PROCEDURE

The experimental setup is shown in Figure 1. The laser operates in two different configurations: a Q-switched oscillator producing 12 ns pulses and a mode locked oscillator producing 35 ps pulses. Separate cavities, each containing a flash-lamp pumped Nd:YAG rod, exist for each configuration. Both cavities produce 1.06 μm pulses at 10 Hz. Before leaving the laser housing, the pulses are incident upon a frequency doubling second harmonic generator[6], which reduces their wavelength to 0.532μm.

The 0.532 μm pulses leave the laser housing with an approximate $1/e^2$ diameter of 1 cm. Since the ZnSe sample has a square face of length 4 mm, the pulse diameter must be reduced in order to avoid overfilling the sample which would result in erroneous measurements for the transmitted intensity.

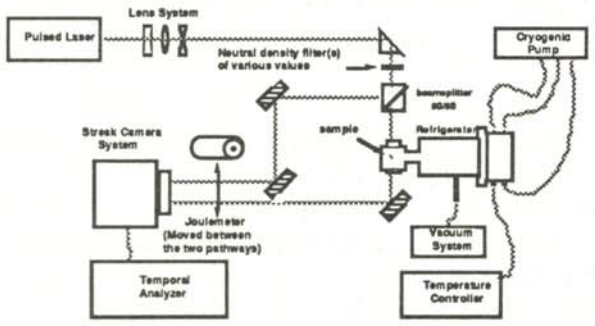

Figure 1
Experimental Apparatus. The laser pulses pass through a lens system, neutral density filters, and a beam splitter. The sample is held in a cryogenic refrigerator. Incident and transmitted energies are read by a joulemeter. Temporal and spatial profiles are measured by a streak camera.

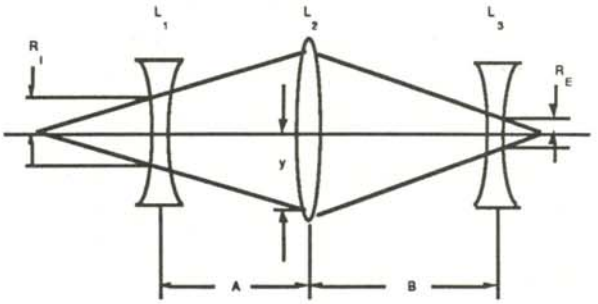

Figure 2
Beam reducing lens system. A diverging - converging - diverging lens configuration reduces the beam diameter without producing an intermediate focal point, which would cause beam attenuation.

A lens system was designed to reduce the beam diameter to 2 mm and to condition the beam's spatial profile. Since the intensity of the pulses was in the MW to GW range, the energy densities of focused pulses would be extremely large and would cause the breakdown of air molecules, plasma formation and subsequent beam attenuation. Therefore, a lens system design with no intermediate focal points was required. A diverging-converging-diverging lens configuration (Figure 2) was used. The design was based on an arbitrary selection of the first and third lenses, which were identical. The focal length of lens 2 was required to be greater than $|F_1|$. Expressions for the minimum diameter of lens 2 and the distance between the lenses was derived by the use of similar triangles and the thin lens formula. Those expressions are:

$$y = \frac{F_2}{F_1}\left[R_I + R_E\right] \tag{7}$$

$$A = F_2\left[\frac{R_E}{R_I} + 1\right] - F_1 \tag{8}$$

$$B = F_2\left[\frac{R_E}{R_I} + 1\right] - F_3 \tag{9}$$

where R_I is the radius of the input beam, R_E is the radius of the output beam, A and B are the distances between the lenses, and y is the minimum diameter of lens 2.

Neutral density filters were used to vary intensity

of the smaller diameter pulsed beams which were then divided by a beamsplitter into two identical beams, each with half the energy of the initial beam. One beam passed through the sample while the other was directed around the sampleholder with mirrors. The energies of the incident and transmitted beams were read by a joulemeter (see below) which was placed first into the path of the incident beam, and then moved to read the transmitted energy. As the joulemeter did not make simultaneous readings of the incident and transmitted energies, the pulse-to-pulse stability of the laser was critical. This stability was verified using the streak camera system.

The joulemeter contains a 5mm pyroelectric crystal connected in parallel with an RC circuit. When a pulse of light is incident upon the joulemeter, the generated heat is converted by the crystal into an electric current. The result is a current source in parallel with an RC circuit which produces an output voltage whose peak amplitude is proportional to the energy contained in the incident pulse. The proportionality factor, or voltage responsivity, is expressed in units of volts per joule. The joulemeter had a factor of 2.77 V/mJ with an uncertainty of ±5%. Joulemeter readings were taken from a 500 MHz oscilloscope. After a pair of energy readings were taken, the joulemeter was removed from the beam line and the laser pulses were collected by the slit and input optics of the streak camera.

In the streak camera (see Figure 3), a slit image of

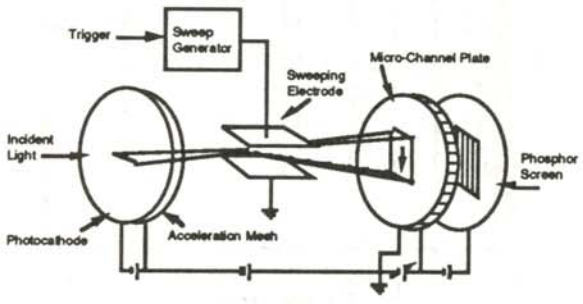

Figure 3
Streak camera operation. A photocathode converts the light image of a pulse into an electron image. A ramp voltage applied to the electrodes sweeps the electron image. A micro-channel plate amplifies the image onto a phosphor screen which converts it back into a photon image.

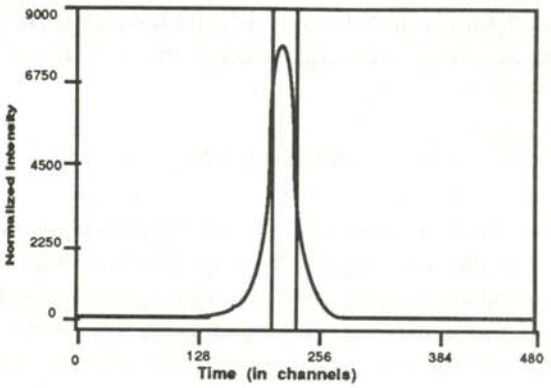

Figure 4
Temporal-analyzer output. A temporal view of a pulse is shown. The number of channels in the FWHM (parallel vetical lines) is divided by 480 and multiplied by the streak time to give the FWHM temporal length

the incident light is formed on a photocathode plane which converts the photon image into an electron image. This electron image is accelerated by an electrode mesh into region where it triggers a high speed ramp voltage which is applied to a pair of deflecting electrodes. This ramp voltage causes the electron image to be swept from top to bottom, across a micro-channel plate. There it is amplified and applied to a phosphor screen which converts the streaked electron image back into a photon image. The light image is detected by a video camera and sent to the temporal-analyzer as image data. The result is a temporal view of a pulse in which the time axis is directed from top to bottom. The sweep times available range from 1 msec to 0.3 nsec. The best time resolution is better than 2 psec.

The streak image produced by the video camera is digitized and inputted into the 512 x 480 x 16 bit frame memory of the temporal-analyzer. A 68000 microprocessor is used to perform analysis of the stored data. A program was used to obtain the FWHM pulse length in number of channels. To convert the number of channels to time the FWHM channels are divided by 480 (the number of temporal channels in the entire streak) and multiplied by the total streak time. In order to obtain the spatial FWHM dimension, the slit of the streak camera was opened all the way and the full image of the pulses were input to the temporal analyzer without

being streaked. The same procedure used to obtain the temporal dimension yields the spatial dimension. A sample of output data from the temporal-analyzer is shown in Figure 4.

RESULTS

The beam parameters were obtained with 12 ns and 35 ps pulses at both room temperature and at 10 K. A computer program was used to combine the four sets of parameters (using equation 6) into input and output intensities. Errors were attributed to each factor. The greatest source of error resulted form the uncertainty in reading the oscilloscope because of jitter in the joulemeter output. The propagation of error was calculated using the form:

$$\text{If } c = a\,b, \text{ then } \sigma_c = c\sqrt{\left[\frac{\sigma_a}{a}\right]^2 + \left[\frac{\sigma_b}{b}\right]^2} \quad (10)$$

The required plots were made with a plotting program. Second order polynomial least squares fits were obtained for I_{out} vs I_{in} plots. The I_{in}/I_{out} vs I_{in} plots yielded straight line fits from which the required slopes and intercepts were read. The plots obtained with the sample at room temperature using picosecond pulses are shown here. The results for all four sets of data are shown in Table 1.

DISCUSSION

Plots of output intensities vs input intensities produced curves which curve slightly downward when I_{in} is increased. This is in accordance with the predicted transmissive behavior of the sample. The plots of I_{in}/I_{out} vs I_{in} are straight lines, in accordance with the solution of the absorption model

Conditions (2mm sample)	α (cm^{-1})	β (cm/GW)
Nano 300K	0.814	0.428
Nano 10K	0.707	0.109
Pico 300K	0.370	0.0645
Pico 10K	0.530	0.01376

Table 1
Absorption coefficients for ZnSe.

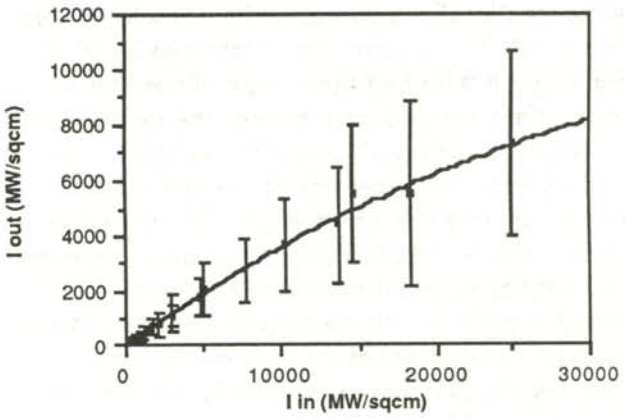

Figure 5
Output intensity vs input intensity for pico-second pulses at room temperature.

(Eqn. 3.)

One would expect the nonlinear absorption coefficient to decrease as the temperature and pulse duration are decreased, since it was postulated that under these conditions other nonlinear effects would be minimized. The results indicate that the nonlinear coefficient did decrease under both conditions. Furthermore, it can be seen that the change in temperature at a particular pulse length had less effect than the change in pulse length at a particular temperature. Therefore, it is concluded that the pulse

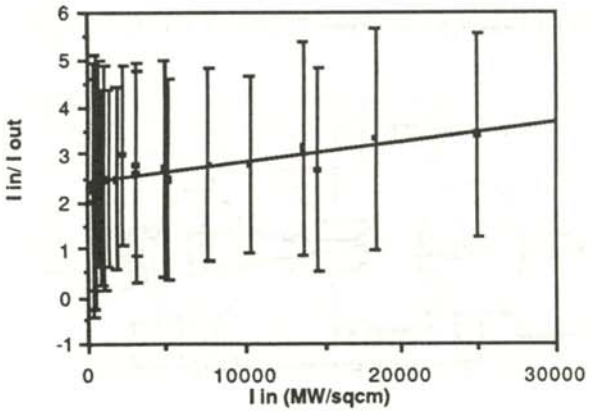

Figure 6
The ratio of input intensity to output intensity as a function of input intensity for pico-second pulses at room temperature. This straight line is in agreement with the solution of

duration is a more critical variable in determining the 2PA coefficient and that in this study, two step absorption is a more predominant effect than absorption due to the generation of free carriers.

The spread in the values of β for ZnSe and for other compounds found in other journals varies by many orders of magnitude[7]. The figures reported in this paper differ by two orders of magnitude from the work of Van Stryland et al[1] who used pulses of approximately 38 psec at room temperature. They report a 2PA coefficient for ZnSe of 5.5 cm/GW and a theoretical ß of 4.27 cm/GW.

ACKNOWLEDGEMENTS

The author would like to thank David J. Kosan and Marc C. Martin of the Air Force Wright Aeronautical Laboratories, Materials Laboratory, and Dr. Jerry Clark of Wright State University, for their assistance and enlightening discussions during the course of this project. The author would also like to thank the Southwestern Ohio Council for Higher Education for the opportunity to work on the project at the Materials Laboratory.

REFERENCES

1) E.W. Van Stryland, et al. Optical Engineering, 24, 4 (1985).

2) N. Peyghambarian and H. M. Gibbs, Journal of the Optical Society of America, 2, (1985).

3) J.I. Pankove, Optical Processes in Semiconductors, Dover Publications, Inc., New York (1971).

4) D. Long, Energy Bands in Semiconductors, Interscience, New York (1968).

5) R.B. James and D.L. Smith, IEEE Journal of Quantum Electronics, 18,11 (1982).

6) A.I. Siegman. Lasers, University Science Books, Mill Valley Calif. (1986).

7) B. Bosacchi et al. Journal of Applied Physics, 49 (8), (1978)

FACULTY SPONSOR OF THIS PAPER

Dr. Jerry Clark
Department of Physics
Wright State University
Dayton, OH 45435

DETERMINATION OF THE TEMPERATURE DEPENDENCE OF THE BAND GAP ENERGY OF A GaAs LED FROM MEASUREMENTS OF ITS EMISSION SPECTRA

Zhen-Hong Zhou
Department of Physics
Polytechnic University
Brooklyn, NY 11201

ABSTRACT

We measured the temperature dependence of the band gap energy of a GaAs Light Emitting Diode (LED) by measuring its emission spectra as a function of temperature between 300K and 360K. We found a linear dependence on temperature with a slope of -0.45 x 10^{-3} eV/K. This agrees well with the empirical fit expression. By comparing the measured and calculated emission spectra, we have shown the effect of the band tails resulting from the heavy doping in the LED. We have also shown that measurement of the emission spectra is a useful method to study the band structure of light emitting semiconductors.

INTRODUCTION

Since the invention of the transistor in 1948 [1], semiconductor technology has grown tremendously. Part of this growth is seen in the invention of semiconductor photonic luminescence devices: the Light Emiting Diode (LED) and the Diode Laser.

As this technology improved, semiconductor LEDs have becomes one of the most important light sources for fiber-optical communications systems[2]. LED's are used for a variety of applications, including lamps, displays, and optoisolators [3]. Since semiconductor light emitting devices are compact, cheap, long lived, and easy to operate, they are a crucial component for future optical computers [4].

LED's use a semiconductor p-n junction for the production of light. Optical radiation is obtained by injecting minority carriers (electrons) into the junction where radiative transitions take place. When the electrons move from the n-side to the p-side of the junction, they recombine with holes, producing photons by spontaneous emission. A similar process produces photons when holes move from the p-side to the n-side and recombine with electrons. The fact that optical emissions are caused by a current make them very easy to modulate.

THEORETICAL BACKGROUND

The theory of semiconductor LED's was developed and compared with optical experiments in the mid

The author received his undergraduate degree in electrical engineering and physics. This paper is based on his bachelor's thesis which won the 1989 SX senior research award. He is going to pursue a Ph.D. in solid state physics, materials and devices at MIT.

1960's [5,6]. The theoretical description of how the bandgap depends upon temperature is less well developed. A detailed review of the theory can be found elsewhere [7,8].

Electron Transition Rate [9]

The electron transition rate determines the emission efficiency as well as the light intensity of a device. It is the foundation needed to calculate the emission spectrum of the LED.

When an electron in the conduction band falls down to the valence band, it gives off a photon whose energy is approximately equal to the bandgap energy (E_g). The bandgap energy is the separation between the energy of the lowest conduction band (E_c) and that of the highest valence band (E_v). This process is called spontaneous emission. The rate at which these transition occur [R_{spon}] depends on the density of state as well as other factors:

$$R_{spon} = C\, f(E_c)\ \{1 - f(E_v)\} \qquad (1)$$

where $f(E_c)$ is the probability that the conduction band contains an electron and $\{1 - f(E_v)\}$ is the probability that a state in the valence band contains a hole (doesn't contain an electron). $f(E_c)$ and $f(E_v)$ are Fermi-Dirac distribution functions for free electrons. C is a constant related to Einstein's B coefficient:

$$C = 8\pi \left(\frac{n}{hc}\right)^3 \left(\frac{h\omega}{2\pi}\right)^3 B \qquad (2)$$

where B is the probability that a transition can occur. It depends on the transition rule and the interaction between the electron and electromagnetic radiation. B can be obtained quantum mechanically by solving the time-dependent Schrödinger equation.

Theoretically Calculated Spectrum

The probability per unit time that an electron at the bottom of the conduction band can spontaneously recombine with holes at the top of the valence band is given by C in Equation 2. The recombination can occur with the emission of a photon. Because the stimulated emission rate for a LED is small, we will not have to take it into consideration.

The radiation field $P(\omega)$ is the product of the spontaneous recombination C, the energy of the photon $h\omega$ and the density of electrons in the conduction band $n(E_c)$ and the density of the holes in the valence band $p(E_v)$ [10]:

$$P(\omega) = G\,\omega^2 \{-E_v\}^{\frac{1}{2}} \{E_c - E_g\}^{\frac{1}{2}} \times \frac{1}{1 + \exp\frac{(E_c - E_{fc})}{kT}} \times \frac{1}{1 + \exp\frac{-(E_v - E_{fv})}{kT}} \qquad (4)$$

where E_{fc} and E_{fv} are the quasi-Fermi levels. The Fermi energy (E_f) is defined as the highest occupied state at 0K. In LED's, where the material is heavily doped, the Fermi energy level splits into two, one in each band called quasi-Fermi levels. E_{fc} and E_{fv} are the quasi-Fermi levels in the conduction band and the valence band respectively. Both E_{fc} and E_{fv} can be calculated from the free electron concentration and the free hole concentration. The constant G in equation 4 is given by:

$$G = \frac{256\,\pi^3}{h^4} (m_h\, m_e)^{\frac{3}{2}} \frac{4\,\pi\, n_o\, q}{h^2\, c^3\, m^2} |M|^2 \qquad (5)$$

where m_h and m_e are the effective masses of holes and electrons in the material respectively, M is the matrix element from quantum mechanics and n_o is the free electron concentration.

Equation 4 is the radiation field of a LED as a function of frequency. This function generates an emission spectrum of the LED by proper selection of the parameters in the equation. A detailed development of Equation 4 can be found elsewhere [11].

Bandgap Temperature Dependence [12]

One of the most striking features of LED's is their frequency tunability. Tuning can be accomplished by altering the temperature of the LED, which leads to changes in the size of the bandgap energy. To understand how temperature affects the bandgap, a variety of optical experiments have been done. The relevant measurements include reflectance [13] and absorption [14,15] at temperatures from 4K to 973K.

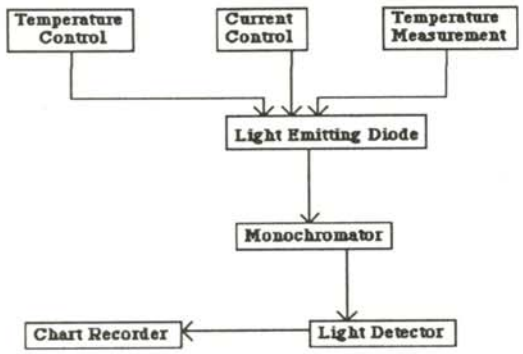

Figure 1
Experimental configuration for measuring the temperature dependence of the bandgap energy of GaAs.

From a large amount of experimental data, Panish and Casey developed an expression based on the empirical fit of their own absorption edge data ($300K < T < 937K$). This linear temperature dependence of the bandgap energy is given by the expression [16]:

$$E_g(T) = E_g(0) - aT^2 / (T + b) \qquad (6)$$

where a and b are constants that depend upon the material. For GaAs, $E_g(0)$ is 1.519 eV, a is 5.405×10^{-4} and b is 204 if T is in Kelvin [16].

In the temperature region between 300K and 360K, where we did our experiment, Equation 6 can be approximated by a linear function of temperature with a slope of -4.6×10^{-4} eV/K.

THE EXPERIMENT

We measured the emission spectrum (power output as a function of wavelength) of a GaAs LED at known driving current in the temperature range between 300K and 360K. Our experimental data agreed well with the linearization of Equation 6 except that the intercept was 1.415 eV instead of 1.519 eV.

The GaAs LED was mounted in a 0.25 inch thick aluminum block which could be heated by a resistor connected to a DC power supply. The temperature was measured using an iron-Constantan thermocouple with a precision of 1K. The experimental configuration is shown in Figure 1.

The injection current was fixed at 19.25 mA. To determine how the bandgap energy depends upon temperature, we measured the spectrum (the power output as a function of wavelength) at different temperatures. The block in which the LED was mounted was heated to a desired temperature, and then the heating current was reduced until the temperature became stable.

The effect of the injection current on the LED was determined by measuring the output intensity of the LED as a function of the diode injection current. The results, shown in Figure 2, were done at room temperature and at a fixed wavelength of 938.6 nm. The injection current was varied from 2.33 mA to 19.25 mA. There did not appear to be a threshold injection current required for a LED. The emission intensity of the LED was linearly dependent upon the injection current.

Keeping the same setup, we recorded twenty spectra, two at each temperature, by scanning the monochromator both ways between 900 nm and 990 nm. Three of the recorded spectra, at temperatures of 300K, 309K and 318K, where sampled and plotted in Figure 3. The wavelength where the corresponding output intensity is maximum (emission wavelength) at the three different temperatures were shifted. As the temperature increased, the emission wavelengths of the LED increased and the relative output intensity decreased.

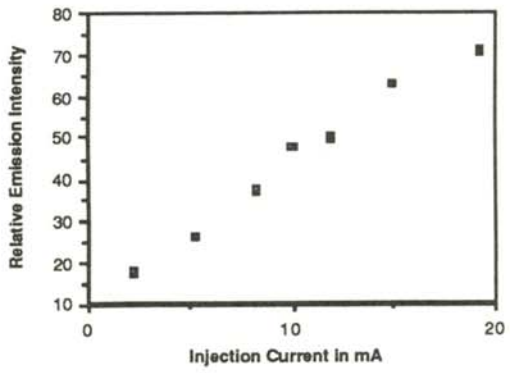

Figure 2
Emission intensity of the LED as a function of injection current. There is no threshold current observed.

The energy of the photon that has the emission wavelength is approximately equal to the bandgap energy. Therefore, we can experimentally determine the bandgap energy at any temperature by measuring the spectrum at that temperature.

DISCUSSION

Experimental Results

We made the observation that as temperature increased, the emission wavelength of the LED increased. The wavelength changes were caused by the change in the size of the bandgap. As the temperature increased, the width of the bandgap decreased, the photon energy decreased, and the emission wavelength shifted to a larger value.

We also found that the LED emits light without a threshold injection current requirement and that the emission intensity is directly proportional to the size of the current. This differs from a laser diode. The difference between the LED and the laser diode can be understood by considering the three basic optical processes which can occur in a semiconductor: absorption, spontaneous emission and stimulated emission. In an LED, spontaneous emission is the dominant transition process, the electrons causes the emission of a photon as it moves from the conduction band to the valence band. The transition rate is independent of how many electrons are available. For the laser diode, stimulated emission is the dominant process. Emission takes place when a photon, whose energy precisely equals that of the bandgap, induces a conduction band electron to make its transition to the valence band. In order to make a laser function, a minimum amount of such photons must be available to induce more electronic transitions, causing the laser diode to have a threshold current.

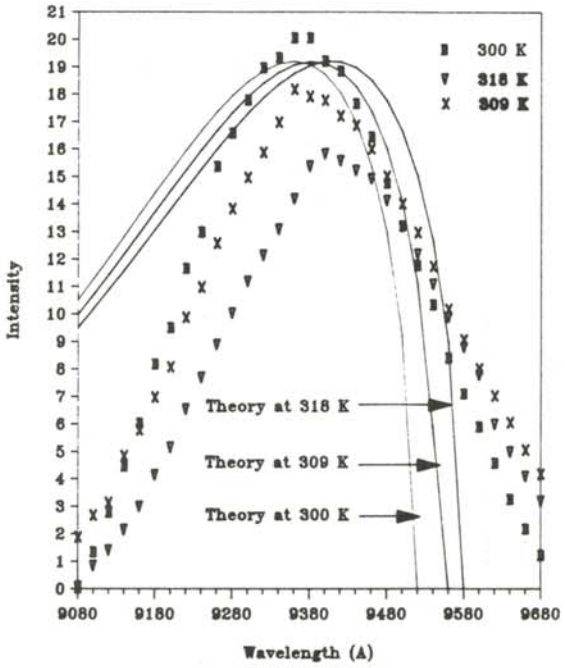

Figure 3

Comparisons between experiment and theory at different temperatures. As the temperature increased, the emission wavelength increased, showing that the bandgap energy decreased.

Theoretical Results

To generate a theoretical spectrum, we chose the quasi-Fermi levels as $E_{fc} = E_g + 0.005$ eV and $E_{fv} = -0.0118$ eV [17]. For intrinsic GaAs, we used $E_g = 1.424$ eV. These values, placed in Equation 4 gave a spectrum which has a peak value at a wavelength of 860 nm. That was consistent with the wavelength emitted by intrinsic GaAs diodes.

This equation shows that the shift in the wavelength of the calculated spectrum is directly proportional to the change in the size of the bandgap energy. To make the calculated spectrum match our experimental results, we had to decrease E_g to 1.305 eV. This bandgap energy is 0.1 eV less than that for intrinsic GaAs at room temperature.

Comparison Between Experiment and Theory

Our experimental and calculated best-fit spectrum is shown in Figure 4. Focus on the right hand side of the peak in Figure 4. Our calculated spectrum, which used parabolic bands for intrinsic GaAs diodes, falls down sharply between the peak value and the maximum wavelength (low energy side of the spectrum). Our experimental spectrum falls down less sharply in the same region. This difference shows that there must be band tails involved in our GaAs sample [18,19]. The sharply falling theoretical curve resulted because we did not take into consideration the band tailing effects in Equation 4.

The band tail is the "tail-like" distribution of states that extends into the forbidden band from either the bottom of the conduction band or the top of the va-

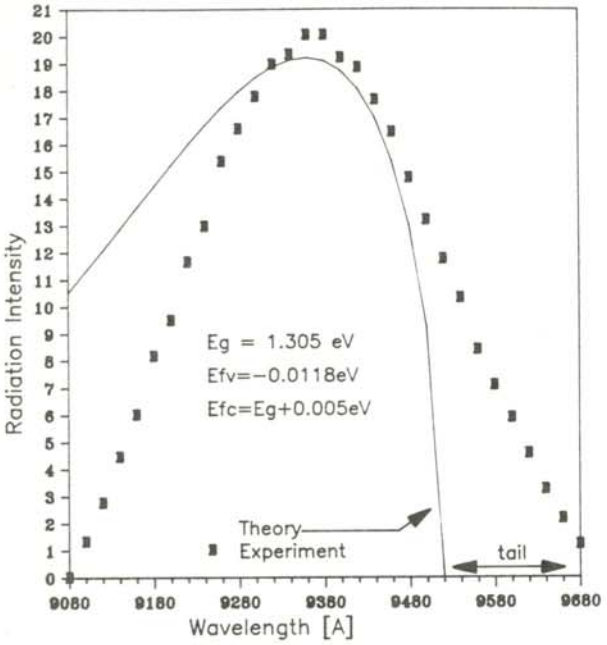

Figure 4
A comparison of the experimentally measured spectrum with the theoretically calculated spectrum of the GaAs LED at 300K. By varing E_g in Equation 4 until the peak of the theoretical spectrum matched that of the experiment, we determined the effective bandgap energy to be 1.305 eV. The emission wavelength is 936 nm and the size of the band-tail is approximatgely 0.048 eV

lence band. The "tail" comes about by the combined effects of many impurity atoms located quite close to one another in a heavily doped semiconductor. The size of the tail is the energy difference between the minimum energy of Equation 4 and that of the experiment shown in Figure 4. The difference of 0.048 eV represents the size of the band tails.

The left hand side (the higher energy side of the spectrum) of the calculated curve falls down much slower than the experimental curve shown in Figure 4. This is due to self-absorption in the GaAs LED. The degree of absorption which occurs depends on the frequency of the light and the semiconductor material being studied. The absorption increases as the frequency of the light increases, At shorter wavelengths, more photons are absorbed, leading to a decrease in emission intensity. Consequently, the experimental curve vanishes faster than the calculated curve.

Substituting the accepted expression for the bandgap temperature dependence of Equation 6 into Equation 4 and varying the temperature gives rise to Table 1. We found that the rate of emission wavelength shift with temperature of 0.3 nm/K of the experimental spectrum agrees with that of the theoretical calculations. Converting the emission wavelength to bandgap energy dives a rate of change of the bandgap energy with temperature to be -0.45×10^{-3} eV/K. This agrees with the linearization of Equation 6 which predicts a slope of -0.46×10^{-3} eV/K.

As shown in Figure 5, our experimental data agree well with Equation 6 if $E_g(0)$ is assigned a value of 1.415 eV instead of the accepted value of 1.519 eV. The need to reduce the bandgap energy by 0.1 eV in order to fit well our experimental data suggests that impurity levels (donor and acceptor levels) may exist in the gap, shrinking it by 0.1 eV. Other possible explanations involve "excitons" [20] (correlated pairs of electrons and holes) or the long range Coulomb interaction between electrons and

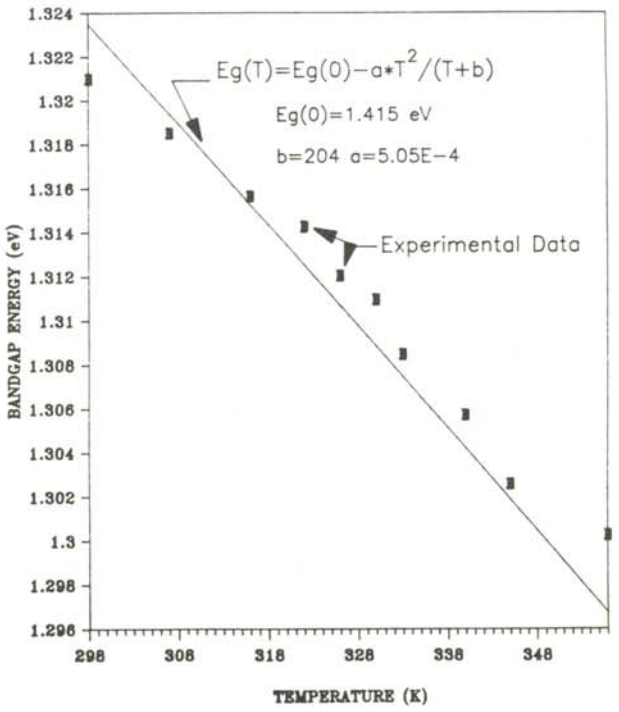

Figure 5
Comparison between the measured and the empirical fit expression of bandgap energy as a function of temperature.

Temperature K	Peak Wavelength in Angstroms Theoretical	Experimental
300	9360	9403
309	9384	9420
318	9408	9440
324	9424	9450
328	9436	9466
332	9447	9474
335	9456	9492
342	9475	9512
347	9490	9535
358	9520	9552
Average Rate (A/K)	2.7	3.0 ± .2

Table 1
Theoretical and experimental values for the emission wavelength as a function of temperature.

holes [21].

CONCLUSION

The magnitude of the effective energy gap shrinkage of a GaAs LED was determined by comparing the calculated emission spectra with the corresponding experimental spectra and finding the energy shifts which give the best fit. The rate at which the peak wavelength of the spectrum shifts with temperature in the range $300K < T < 360K$, is -0.45×10^{-3} eV/K, This agrees well with the accepted empirical fit expression of Equation 6. These results indicate that the measurement of the emission spectrum is a useful method of studying the band structure of light emitting semiconductors.

ACKNOWLEDGMENTS

The author would like to thank Dr. Donald Scarl of Polytechnic University for his constant guidance and encouragement. His superb skills enabled the accomplishment of this work.

REFERENCES

1. S.G. Burns and P.R. Bond, Principles of Electronic Circuits, West Publishing Co., New York, 1987.
2. Tingye Li, "Lightwave Telecommunication", Physics Today, May 1985, pp 24-31.
3. S. Gage, D. Evans, M. Hodapp, and H. Sorenson, Optoelectronics Applications Manual, McGraw-Hill, New York, 1977.
4. S.M. Sze, Physics of Semiconductor Devices, Wiley, New York, 1981.
5. G. Burns and M.I. Nathan, Proc. IEEE, 52, July 1964, pp. 770-794.
6. R.H. Rdiker, "Semiconductor Lasers", Physics Today, 18, Beg 1966, pp. 542-554.
7. M.I. Nathan, "Semiconductor Lasers", Proc. IEEE, 54,10, Oct 1966.
8. R.Y. Yang, Measurement of Temperature Dependence of Diode Laser Wavelength, Ph.D. Dissertation, Polytechnic University, New York, 1987.
9. J.S. Blakemore, Gallium Arsenide, Key Paper in Physics, #1, A.I.P., New York, 1987.
10. R.H. Bube, Electrons in Solids, Academic Press, new York, 1981.
11. Z.H. Zhou, Measurements of the Bandgap Temperature Dependence of a GaAs LED From Its Emission Spectra, Bachelor's Thesis, Polytechnic University, New York, 1989.
12. H.C. Casey, Jr. and M.B. Panish, Hetro-Structure Lasers, Part A: Fundamental Principles, Academic Press, New York, 1978.
13. D.D. Sell, Phys. Rev., B6, 1972, P. 3750.
14. M.D. Sturge, Phys. Rev., 127, 1962, p. 786.
15. M.B. Pansih and H.C. Casey, J. Appl. Phys. 40, 1969, p. 163.

16. C.D. Thurmond, "The Standard Thermodynamic Functions for the Formation of Electrons and Holes in Ge, Si, GaAs, and Gap", J. Elect. Soc:Solid-State Sci. Tech., 122, 8 Aug. 1975, pp. 1133-1141.

17. G. Lasher and F. Stern, "Spontaneous and Stimulated Recombination Radiation in Semiconductors", Phys. Rev., 2A, 133, Jan. 1964, pp. 553-563.

18. C.J. Hwang, Calculation of Fermi energy and Bandtail Parameters in Heavily Doped and Degenerate n-type GaAs", J. Appl. Phys., 41,6, 1970, pp. 2668-2674.

19. C.J. Hwang, "Properties of Spontaneous and Stimulated Emission in BaAs Junction Lasers", Phys. Rev, 2B, 10, Nov. 1970, p. 4117.

20. K. Cho, Excitons, Springer-Verlag, Berlin, 1979.

21. L.D. Laude, Cohesive Properties of Semiconductors under Laser Irradiation, Martinus Nijhoff Publishers, Boston, 1983,

FACULTY SPONSOR

Dr. Donald Scarl
Department of Physics
Polytechnic University
Farmingdale, NY 11735

UNUSUAL PROCESSES IN THE ELECTRON IMPACT IONIZATION OF 1,2 DICHLORO-ETHANE

Zoran Psenicnik
Department of Physics
Laboratory for Solid State Science and Technology
Syracuse University
Syracuse, NY 13244

ABSTRACT

The ionization potential of a molecule can be measured using electron impact mass spectroscopy by recording an ionization efficiency curve (IEC). When the IEC of 1,2 dichloro-ethane ($C_2H_4Cl_2$) was recorded, an unusual peak-like structure was observed well below the ionization potential. This anomaly in the ionization of 1,2 dichloro-ethane can be explained by ion-molecular collisions and invoking a long-lived metastable state. Previously unidentified optical absorption features for the same molecule are connected to this postulated long-lived metastable state. The details of these measurements, with emphasis on instruments and data acquisition, are discussed as well.

INTRODUCTION

One of the incentives to perform a study of 1,2 dichloro-ethane was the technological importance of that molecule. 1,2 dichloro-ethane is the major starting material in the production of vinyl chloride (VC) which is widely used in the synthesis of polyvinyl chloride (PVC).

The main process used to produce VC is the dehydrochlorination (removal of HCl) from 1,2 dichloro-ethane[1].

$$C_2H_4Cl_2 \rightarrow CH_2{=}CHCl + HCl \qquad (1)$$

Zoran Psenicnik came to the United States as a high school exchange student from Yugoslavia. He was addmitted to Syracuse University with a full scholarship. He is a double major in physics and engineering.

The large ionization cross-section of this molecule makes it very suitable for electron impact studies in a mass spectrometer. In the ion source of a mass spectrometer, electrons with sufficient kinetic energy incident upon a stream of the desired gaseous species, will create positive ions. This process is similar to a plasma, where positive ions are created from the gas as a result of the impact of electrons on neutral gaseous molecules. What is particularly interesting about this ionization process is that for 1,2 dichloro-ethane, it appears to be influenced by ion-molecular collisions. Long lived excited states of the gaseous molecule can have a profound influence upon the gaseous chemistry of that molecule.

In particular, long lived excited states of a molecular species can result in a plasma composition strongly influenced by second and third order reactions and not just first order fragmentation and recombination processes. These long lived excitations

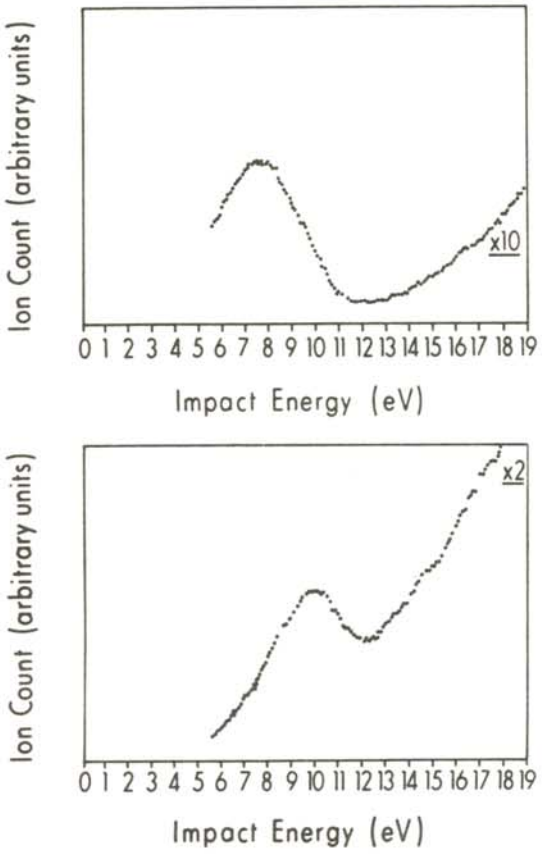

Figure 1

Ionization efficiency curves for $C_2H_4Cl_2^+$ (top) and its major fragment $C_2H_3Cl^+$ (bottom)

may provide states suitable for collision induced pathways for ionization of the parent species.

Full understanding of the ionic and neutral decomposition will enable us to postulate the plasma assisted fragmentation pathways leading towards production of vinyl chloride. This will open new possibilities in technological development of plasma assisted chemistry.

THE EXPERIMENT

We investigated the electron impact ionization of 1,2 dichloro-ethane using the electron gun of a mass spectrometer to ionize 1,2 dichloro-ethane gas and measuring the ion production as a function of the electron impact energy. The ion yield intensity's dependence upon electron impact energy is called the ionization efficiency curve (IEC).[2]

The IEC, above the threshold, is linearly dependent upon the impact energy [3], therefore, by extrapolation back to the origin of the energy axis, one can determine the threshold energy for ionization. This threshold is called the ionization potential (IP) of the ion or the appearance energy (AP) if one is detecting a fragment ion.

Ionization by electron impact can be used to calculate the bond strength, the relative abundance, and various thermodynamic cycles. The bond strength $D(X\text{-}Y)^+$ is given by:

$$D(X\text{-}Y)^+ = AP(Y)^+ - IP(X)^+ \qquad (1)$$

where $IP(X)^+$ is the ionization potential of the parent ion and $AP(Y)^+$ is the appearance potential of the fragment ion.

The IEC for 1,2 dichloro-ethane, seen in Figure 1, shows unusual peaks below the ionization potential. Our postulate that this effect was caused by ion molecular collisions involving a long lived meta stable state was confirmed by photoionization measurements on 1,2 dichloro-ethane and other simple gaseous haloforms. These results indicate the existence of such a state at 4 eV.

Mass Spectroscopy

A mass spectrometer is an instrument which creates a beam of gaseous ions from a desired sample, uses a magnetic field to analyze them according to their mass-to-charge ratio (m/q) and finally produces a signal which is a measure of the relative abundance for each ionic species. The m/q value is the ratio of the sum of the mass numbers of the atoms composing the particular molecule divided by the number of electrons lost during ionization. Even though most of the molecules in mass spectrometry experiments are singly ionized, atoms and some molecules may lose more than one electron without disintegration or decomposition [4,5,6].

When a singly ionized particle of charge q and velocity $\bar{v}$ is introduced into the magnetic field ($\bar{B}$) of the mass spectrometer, it experiences a force $\bar{F}_B$:

$$\bar{F}_B = q\,(\bar{v} \times \bar{B}) \qquad (2)$$

Since the magnitude of $\bar{B}$ and $\bar{v}$ do not change while the particle moves, the magnitude of the $\bar{F}_B$

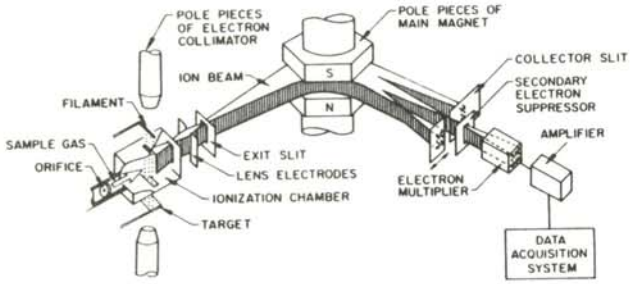

Figure 2
Schematic diagram of a single focus magnetic sector mass spectrometer (Hittachi RMU-6E)

is constant. Under the influence of a force with a constant magnitude and directed perpendicular to the velocity, the orbit of the particle becomes a circle. Therefore, we know that:

$$F_B = Bev = F_c = mv^2/r_m \qquad (3)$$

where r_m is the radius of the orbit.

If the charged particles are accelerated through a potential difference V, they will form an ion beam homogeneous in energy where:

$$E_K = 1/2\ m\ v^2 = V\ q \qquad (4)$$

Combining Equations 3 and 4 gives:

$$m/q = B^2\ r_m^2\ /\ 2V \qquad (5)$$

For our instrument, (shown schematically in Figure 2) with a fixed ion collector and hence a fixed value of r_m, one is able to achieve selection of successive ions with a specific m/q ratio by scanning the spectrum. This scanning is accomplished by either varying V or B. Increasing the magnetic field or decreasing the accelerating potential will focus heavier ions into the collector.

Ions are created in the mass spectrometer's ion source by collisions between neutral molecules and electrons produced by thermal emission from the hot filament. By controlling the potential difference (V_c) between the filament and the rest of the chamber, electrons can be accelerated across the incoming gas stream and acquire a kinetic energy:

$$E_c = e\ V_c \qquad (6)$$

where E_c is the electron impact energy.

The value of E_c determines the ion yield in the ion source. As shown in Figure 2, the ions produced are then accelerated through the potential difference, pass through the exit slits (which collimate the ion beam) and into the magnetic field. By varying the magnetic field, we focus ions with different m/q rations into the detector (an electron multiplies). The observed ion current is amplified and sent to a chart recorder.

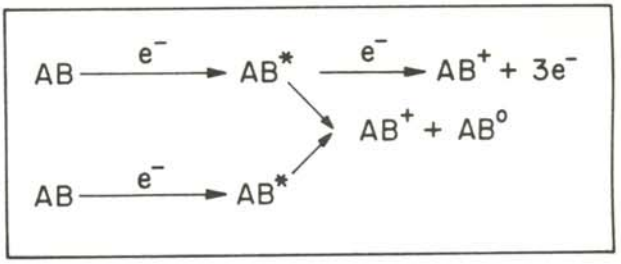

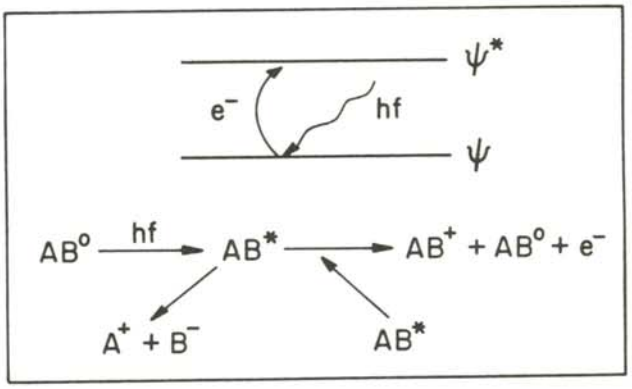

Figure 3
Ionization processes with metastable intermediate states.
Top
Ions (AB^+) can be created by mutual collisions of excited states (AB*) or additional collisions with electrons (e-).
Bottom
Neutral molecule (AB^o) upon the absorption (Ψ -> Ψ^*) of incident radiation (hv) can dissociate creating positive and negatiave fragments, or after collisions of excited molecules,

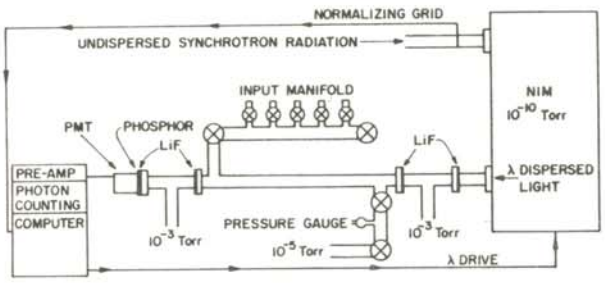

Figure 4
Schematic diagram of the set up used for the photoabsorption experiment.

The gas phase electron impact measurements presented in this paper were performed on a single focus magnetic sector mass spectrometer, differentially pumped by two diffusion pumps [7]. The ionization efficiency curves were recorded as a function of impact energy from approximately 5.6 eV to 35.6 eV in 0.1 eV steps. The pressure of the gas could only be measured on a relative scale. The energy scale was calibrated using high purity argon and nitrogen.

Photoabsorption

The absorption of electromagnetic radiation is useful in the study of the one electron transitions in gaseous molecules [8,9]. The energy of a photon is absorbed only if its energy is equal to the energy difference between two available energy levels:

$$h\nu = E_{exc} - E_o \qquad (7)$$

where ν is the frequency of the incident radiation, h is Planck's constant, E_o is the energy of the non-excited state, and E_{exc} is the energy of the excited state. If that excited state is at an energy level higher that the first ionization potential (IP), ionization may occur. It is possible, as shown in Figure 3, to cause ionization in molecular species even if the energy of the photon is less than IP [10].

The photoabsorption spectra for 1,2 dichloroethane and other simple gaseous haloforms were obtained using synchrotron radiation [10]. The light source for this experiment was the electron ring Tantalus at the Synchrotron Radiation Center operated by the University of Wisconsin, Madison. A schematic representation of our apparatus is shown in Figure 4. The light was dispersed by a 1m MacPherson normal incidence monochromator with 600 lines/ inch grating and transmitted through the cell [10,11].

We measured the photon flux passing through a gas cell. The photons were detected by a photon multiplier with a sodium salicylate phosphor. Because the monochromator and the gas vessel were separated by a LiF window, spectra could be obtained only between 2.0 eV and 11.5 eV photon energy. All spectra were taken by sending the pulses into a multi channel data acquisition computer and normalized to a constant photon flux. The data were plotted as a function of $\ln(I_o/I)$, where I_o is the transmitted light intensity of the empty cell and I is the transmitted intensity of the filled cell.

RESULTS

The IEC of $C_2H_4Cl_2^+$ and its major fragment $C_2H_3Cl^+$, shown in Figure 1, exhibit well notice-

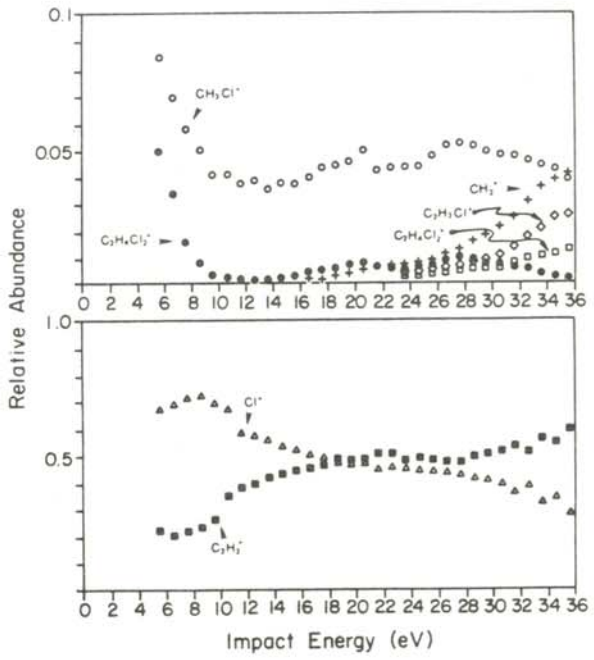

Figure 5
Relative abundance curves for the fragmentation of $C_2H_4Cl_2$

able peak-like structure. This structure was detected for several accelerating potentials.

Figure 5 is the relative abundance curve for the fragmentation of $C_2H_4Cl_2$. The identification of fragment is only tentative due to resolution limits of the mass spectrometer.

Figure 6 represents the photoabsorption spectra for CCl_4, $CHCl_3$ and $C_2H_4Cl_2$, with assigned one electron transitions. The photoabsorption spectra for $C_2H_4Cl_2$ at low photon energy is shown in the insert. The photoabsorption feature observed at approximately 4eV for $C_2H_4Cl_2$ is similar to those noticed at 4 - 4.7 eV for CCl_4 and CCl_3Br as seen in Figure 7.

DISCUSSION

The value for the ionization potential potential of 1,2 dichloro-ethane was extrapolated from the IEC (Figure 1) of $C_2H_4Cl_2$. The value of 11.20±.05 eV is in good agreement with the other results [11].

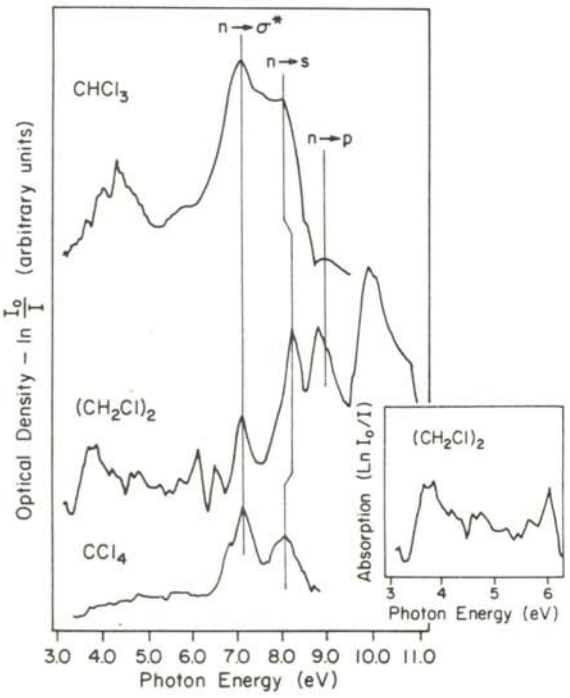

Figure 6
Photoabsorption spectra for CCl_4, $CHCl_3$ and $C_2H_4Cl_2$. The insert shows the photoabsorption spectra for $C_2H_4Cl_2$

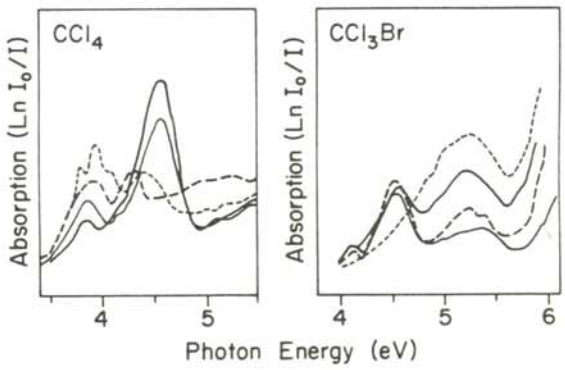

Figure 7
Low energy photoabsorption spectra for CCl_4 and CCl_3Br shwoing similar features as the low energy protoabsorption spectra for $C_2H_4Cl_2$

The existence of a long lived metastable excitation state is also noticeable in the IEC of $C_2H_4Cl_2^+$ and $C_2H_3Cl^+$ where there are broad peaks centered at 7.5 eV and 9.7 eV respectively. The onset of this feature, the low energy peak in the IEC, is about 4 eV.

The photoabsorption spectra of $C_2H_4Cl_2$, CCl_3Br, and CCl_4 (Figure 6) show one electron transitions at 7.2 ev (n -> σ*), 8.0 eV (n -> s) and 9.0 eV (n -> p). Additional photoabsorption features are seen at about 5.0 eV for $C_2H_4Cl_2$ (insert of Figure 6) and at 4.5 eV for CCl_4 and CCl_3Br (Figure 7) which are well below the n -> σ* transition. This photoabsorption feature is consistent with the results seen in the mass spectroscopy data.

These features may be the result of ion pair production or some other fragmentation process dues to the excited metastable state. Evidence from pressure variation measurements suggests that these excitations are collision sensitive. We postulate that the 4.0 eV absorption feature is a result of a long lived metastable state which can be collisionally deexcited.

The peak like structure in the IEC is unusual in that it occurs at an energy below the ionization potential. The ionization process for creating ions at energies below the IP must be a second order process, so that the molecule can attain sufficient

energy to ionize. Such a process requires a long lived excited state as shown in Figure 2. Our results indicate that the excited state is an an intermediate in the direct ion pair production. Since this peak seems to be unaffected by different accelerating potentials, the ionization probably involves collisions of neutrals. According to the relative abundance data, the excited state appears to be related to the fragmentation process. At energies below 10 eV, the most abundant fragment is $C_2H_3Cl^+$, with elimination of neutral HCl. While not conclusive, this suggsts that the excited state is related to the fragmentation process which eliminates neutral HCl.

ACKNOWLEDGMENTS

This work was funded by research awards given to P.A. Dowben of Syracuse Univesity by B.F. Goodrich and by the Fredrickson Fellowship Fund of Syracuse University. The author world like to thank the staff of the Synchrotron Radiation Center of the University of Wisconsin, Madison. The SRC is supported by the National Science Foundation through grant # DMR-80-21888.

REFERENCES

1. M. Sitting, Vinyl Chloride and PVC Manufacture, NDC, 1978.

2. D.C. Frost and C.A. McDowell, Proc. R. Soc. London, Ser.A, 241, 1957, p. 194.

3. D.C. Driscoll, Doctoral Dissertation, Syracuse University, May 1987.

4. G.W.A. Milne, Mass Spectrometry: Techniques and Applications, Robert E. Kreiger, 1979.

5. J. Roboz, Introduction to Mass Spectroscopy, Instrumentation and Techniques, Interscience Publisher, 1968.

6. H.E. Duckworth, R.C. Barber, and V.S. Venkatasubramanian, Mass Spectroscopy, Cambridge University Press, 1986.

7. Y.J. Kime, D.C. Driscoll, P.A. Dowben, J. Chem. Soc., Faraday Trans. 2, 83, 1987 p. 403.

8. J. Berkowitz, Photoabsorption, Photoionization, and Photoelectron Spectroscopy, Academic Press, 1979.

9. C. Kunc, Synchrotron Radiation, Techniques and Application, Springer Verlag, 1979.

10. D.C. Driscoll, J.A. Bishop,, B.J. Sturn, and P.A. Dowben, J. Vac. Sci. Tech., A4(e), May/June 1986.

11. R. Tate, D.C. Driscoll, and G. Stauf, Z., Naturforsch., 41a, May 1986, p. 1091.

12. K. Watanabe, T. Nakayama, and J. Motte. J. Quant. Spectrosc. Radiat. Transfer, 2, pp. 369-382.

FACULTY SPONSOR

Dr. Peter Dowben
Department of Physics
201 Physics Building
Syracuse University
Syracuse, NY 13244-1130

THE MADELUNG ENERGY OF THE SUPERCONDUCTOR $YBa_2Cu_3O_7$ *

Kenneth A. Ritley
Oak Ridge National Laboratory [a]
PO Box 2008
Oak Ridge, TN 37831-6243

ABSTRACT

The Madelung energy (the electrostatic potential energy) of the new high T_c superconductor $YBa_2Cu_3O_7$ was calculated using the method of Ewald. [1] The calculation was demonstrated by first obtaining the Madelung energy of NaCl and the constituent oxides of the superconductor: CuO, Cu_2O, Y_2O_3 and BaO. The electrostatic potential at the individual ionic sites in $YBa_2Cu_3O_7$ was obtained and an explanation for the formation of Cu-O "chains" in the orthorhombic (superconducting) phase of this material suggested. Finally, a variant of the Ewald method was used to determine the electrostatic equipotential lines within an ionic crystal and applied to determine the electrostatic potential around the oxygen vacancy sites in the layer containing the Cu-O "chains" in the superconducting phase of $YBa_2Cu_3O_7$.

1. P.P. Ewald, Ann. der Phys., 64, 1921, p. 253.

INTRODUCTION

There has been much activity regarding the new high T_c superconductors such as the yttrium-barium-copper-oxide $YBa_2Cu_3O_7$. Its molecular structure was recently determined using high resolution neutron powder diffraction techniques. [1] They found it to have an orthorhombic structure with lattice parameters a = 3.8231 Å, b = 3.8864 Å and c = 11.6807 Å. The unit cell of $YBa_2Cu_3O_7$ is shown in Figure 1.

We computed the electrostatic energy for $YBa_2Cu_3O_7$ along with other simple ionic compounds using the method of Ewald [2] as explained in Kittel.[3] To compute the total electrostatic energy of $YBa_2Cu_3O_7$, we assumed that it exists as an ionic crystal with known charges for each of the ions. The procedure we used was quite general and is applicable to calculating the electrostatic binding energies of many ionic compounds.

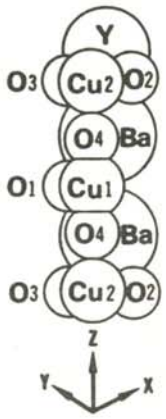

Figure 1
Schematic view of the unit cell (13 atoms) of the high T_c superconductor $YBa_2Cu_3O_7$. The atoms are labeled according to Table 2.

Ken is a graduate of Sonoma State University in Rohnert Park, CA. He is currently a graduate student at the University of Mass. - Amherst.. The past summer he worked at Brookhaven National Laboratory investigating cold fusion.

We also used a variant of Ewald's method to determine the electrostatic equipotential lines within ionic crystals. We applied it to $YBa_2Cu_3O_7$ to determine the electrostatic potential energy in the neighborhood of the oxygen vacancies.

An accepted quantum mechanical description of the mechanisms responsible for superconductivity in this oxide has not been found. Neither is it known to what extent this compound exhibits ionic or covalent bonding. Our calculations were purely classical in nature and did not provide answers to the question of what mechanism was responsible for superconductivity at such high temperatures in this oxide.

THE EWALD METHOD

The electrostatic contribution to the binding energy of ionic crystals is known as the Madelung energy [3,4]. We define the Madelung constant following Pauling [4] as:

$$\alpha = -\sum_i \frac{q_i \psi_i R}{2N} \qquad (1)$$

where q_i is the charge on an ion, ψ_i is the electrostatic potential at the site of ion i due to all other ions in the lattice, N is the number of stoichiometric molecules in the unit cell, and R can be either the nearest-neighbor distance, the lattice parameter (a), or, if the unit cell is not cubic, the cube root of the molecular volume (δ). The sum is over all of the ions in the unit cell. Tables of α for various compounds appear in the literature, [3,4] but the reader is cautioned to note carefully which value of R is used to obtain the results.

The Madelung energy per stoichiometric molecule, U/N is expressed in terms of the Madelung constant (α) as:

$$\frac{U}{N} = -\frac{e^2 \alpha}{R} \qquad (2)$$

where e is the fundamental unit of electric charge. The problem of determining α, and hence the Madelung energy, is reduced to the problem of calculating all ψ_i for a particular ionic solid. In principle, the electrostatic potentials can be calculated from:

$$\psi_i = \sum_{l \neq i} \frac{q_l}{r_l} \qquad (3)$$

where r_l is the distance between the i^{th} and the l^{th} ion and the sum is over all ions l in the lattice. In practice, however, this sum converges too slowly to be of any practical use. To demonstrate this, we computed this sum directly for a positive ion in NaCl, summing terms in order of increasing distance from the ion. We found out that even after 10^5 ions, the sum did not converge to any degree of accuracy. This is demonstrated for a portion of the sum in Figure 2. As successive shells from a given ion are summed, the radius of the shells increase, but the number of ions in any given shell and the charges are always changing. This technique results in the poor convergence of the series.

Several techniques have been devised to make this sum converge more rapidly. [5] A technique developed by Evjen [6] evaluates the above sum in such a way that the sum is taken over shells of neutral charge. This method results in rapid convergence of the series for specific cases, but does not lend itself well to computing the Madelung constant for an arbitrary crystal configuration.

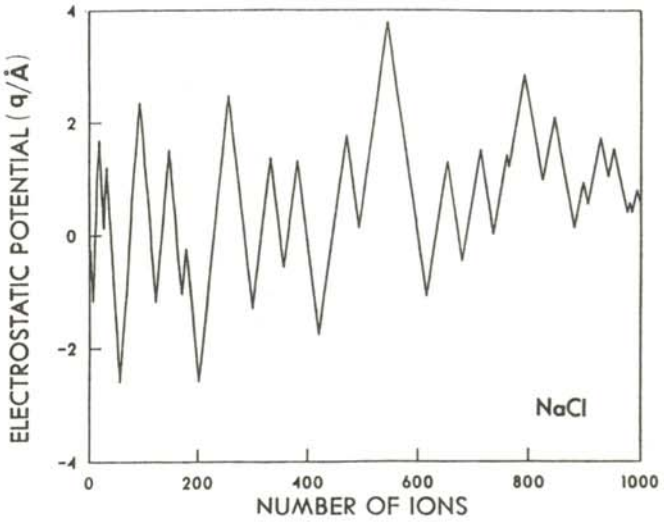

Figure 2
The electrostatic potential (q/Å) vs number of ions for a Na site in NaCl, demonstrating the poor convergence of the general form (Equation 3) of the electrostatic potential.

The most general technique is Ewald's method. [2] We shall not derive the results here, but refer the reader to an excellent derivation in Kittel.[3]

The ions in the lattice are considered to be point charges, giving a lattice of delta functions as the charge distribution. The poor convergence of the sum is improved in the Ewald technique by screening each delta function with a Gaussian charge distribution of equal and opposite charge defined as:

$$\rho_l = q_l \left(\frac{\eta}{\pi}\right)^{\frac{3}{2}} \exp\left\{\frac{-\eta}{r^2}\right\}$$

and (4)

$$\int \rho_l \, dr = q_l \, .$$

The sum of the point charges and oppositely charged Gaussians provide a nearly neutral charge distribution when viewed from a distance, hence improving the convergence. One must, of course, subtract off a sum over the Gaussian distributions to yield the desired sum of the lattice of point charges. Manipulation of these two sums, a lattice of screened delta functions and a lattice of Gaussians, results in a potential composed of three terms - a reciprocal space term, a self term and a real space term:

$$\psi_i = \frac{4\pi}{\Delta} \sum_G S(G)\, G^{-2} \exp\left\{\frac{-G^2}{4\eta}\right\} - 2\, q_i \left(\frac{\eta}{\pi}\right)^{\frac{1}{2}} + \sum_l \frac{q_l}{r_l} \operatorname{erfc}\{\eta^{\frac{1}{2}} r_l\} \qquad (5)$$

where Δ is the volume of a unit cell, **G** represents the reciprocal lattice vectors, and erfc is the complimentary error function. The first sum is over the reciprocal space lattice vectors and the second sum is over the real space lattice vectors. The structure factor, S(**G**), is given by:

$$S(G) = \sum_t q_t \exp\{-i\, \mathbf{G} \cdot \mathbf{r}_t\} \qquad (6)$$

where the sum is just over the ions in the unit cell. The convergence parameter η is an independent constant which determines how much the real space or reciprocal space terms are weighted in the final results. Note, that as η approaches zero, Equation 5 reduces to Equation 3.

THE CALCULATIONS

The basic information necessary for the calculation of ψ_i is a knowledge of the unit cell of the ionic solid in question. The reciprocal lattice vectors are defined in terms of the lattice vectors. If **a**, **b**, and **c** are lattice vectors, the reciprocal lattice vectors **G** are given by:

$$\mathbf{G} = h\,\mathbf{A} + j\,\mathbf{B} + k\,\mathbf{C} \qquad (7)$$

where

$$\mathbf{A} = 2\pi \frac{\mathbf{b} \times \mathbf{c}}{\mathbf{a} \cdot \mathbf{b} \times \mathbf{c}}$$
$$\mathbf{B} = 2\pi \frac{\mathbf{c} \times \mathbf{a}}{\mathbf{a} \cdot \mathbf{b} \times \mathbf{c}} \qquad (8)$$
$$\mathbf{C} = 2\pi \frac{\mathbf{a} \times \mathbf{b}}{\mathbf{a} \cdot \mathbf{b} \times \mathbf{c}}$$

and h, j and k are integers.

Once the positions of the ions within the unit cell and the reciprocal lattice vectors are known, it is a simple procedure to generate the real space and the reciprocal space lattice vectors desired for the computation. Crystal lattice data for NaCl, BaO, CuO and Cu_2O were obtained from Wyckoff.[7] Data for Y_2O_3 and $YBa_2Cu_3O_7$ were taken from Wycoff [8] and Beno et.al. [1] respectively.

We developed a computer program to replicate the structure of the unit cell to obtain the real space and the reciprocal space vectors for use in the computation of the electrostatic potentials of Equation 5. The proper choice of η was essential for obtaining

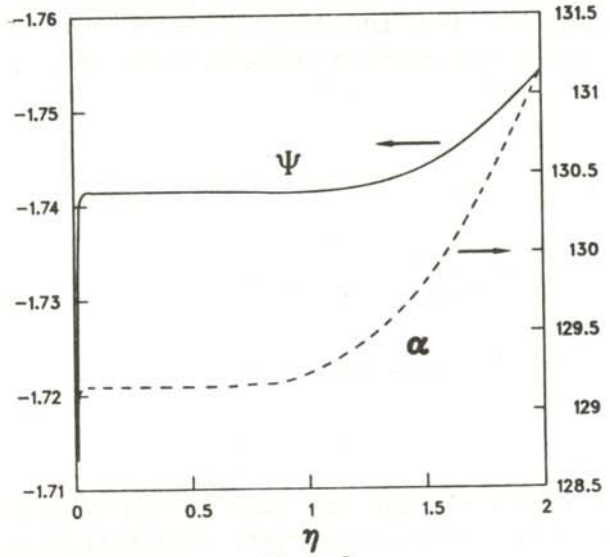

Figure 3

The electrostatic potential, $\psi(\text{Å}^{-1})$, of the yttrium ion in $YBa_2Cu_3O_7$ and the Madelung constant, α, for $YBa_2Cu_3O_7$ vs η.

an accurate result with a fixed number of lattice vectors. Ideally, the potential ψ_i should be independent of η; a graph of η vs ψ_i should be a horizontal line. Because we were considering only finite sums, and had to contend with round-off error, we found that this situation was not the case. Figure 3 shows a plot of the potential for the yttrium ion in $YBa_2Cu_3O_7$. Since α depends on the potentials of all ions in the unit cell, examination of the dependence of α on η is also important. The Madelung constant (α) for $YBa_2Cu_3O_7$ has been plotted as a function of η as the dashed line in Figure 3. For large η, the Madelung constant begins to increase due to a lack of convergence of the reciprocal space term. For $YBa_2Cu_3O_7$, η was chosen to be 0.37.

The computer time required for the computation of α varies widely, depending upon the structure of the solid considered. For NaCl, the calculation of the Madelung energy took roughly 10 CPU seconds on a VAX 8600, while 48 minutes of CPU time were required for Y_2O_3, whose unit cell contains 80 atoms. The Madelung energies of simple ionic crystals can be obtained in a reasonable length of time using an IBM PC-AT.

We found it practical to use on the order of a thousand real space and reciprocal space vectors in the calculation since the computer time required for the calculation was not substantial. However, it is possible to reduce the number of vectors used, provided the terms of the sum are periodically checked to ensure that the series is converging.

ELECTROSTATIC POTENTIAL RESULTS

The calculated Madelung constants and the Madelung energy/molecule for the ionic crystals appear in Table 1. We found values for α for NaCl and Cu_2O in the literature. [4] Our results agree with those given to better than 4 significant digits. The Madelung constant and energy/molecule for the high T_c superconductor are also shown in Table 1.

COMPOUND	ATOMS IN UNIT CELL	MOLECULES IN UNIT CELL	R(Å)	MADELUNG CONSTANT (α)	MADELUNG ENERGY PER MOLECULE (eV)
NaCl	8	4	a = 5.64	3.495	-8.92
BaO	8	4	a = 5.523	13.98	-36.45
Cu_2O	6	2	a = 4.2696	10.23	-34.50
CuO	8	4	δ = 2.7137	9.09	-48.24
Y_2O_3	80	16	a = 10.604	112.7	-153.0
$YBa_2Cu_3O_7$	13	1	d = 5.578	129.2	-333.4

Table 1
Calculated Madelung Energies

The high value for α for the superconductor $YBa_2Cu_3O_7$ is not at all surprising since α depends on the number of atoms in the unit cell and their charges.

Of greater interest than the Madelung energy of the superconductor are the electrostatic potentials for each of the ions in the unit cell. These ionic potentials are a measure of the strength of the electrostatic forces felt by each ion. These results are shown in Table 2 along with the lattice parameters of the ions as determined by Beno et.al. [1]. Note that we have taken a charge of 2.5e on the Cu2 site and a charge of 2.0e on the Cu1 site to maintain charge neutrality.

Of particular interest is the low electrostatic potential obtained for the O1 site oxygen. According to Beno et.al.[1], this oxygen atom has the largest measured thermal ellipsoid (a measurement of the mean square displacement of an atom from its location at absolute zero), indicating that it is the atom which is the least tightly bound.

ELECTROSTATIC EQUIPOTENTIAL LINES

An immediate consequence of the Ewald method, one not mentioned by Kittel, but, we feel, of far greater interest and application is a way to determine the electrostatic potential at *any* arbitrary location within the crystal. The derivation follows from that of Equation 5. Instead of calculating the potential at the origin of a coordinate system, it is calculated at an arbitrary distance r removed from a lattice site. This "perturbed form" of the Ewald potential at a distance **r** removed from site i may be written as:

$$\psi_i(\mathbf{r}) = \frac{4\pi}{\Delta}\sum_{\mathbf{G}} S(\mathbf{G})\, G^{-2} \exp\left\{\frac{-G^2}{4\eta}\right\} \exp\{i\,\mathbf{G}\cdot\mathbf{r}\} - 4\,q_i\left(\frac{\eta}{\pi}\right)^{\frac{1}{2}} + \frac{q_i}{r}\,\mathrm{erfc}\{\eta^{\frac{1}{2}} r\} + \sum_{l}\frac{q_l}{|\mathbf{r}_l - \mathbf{r}|}\,\mathrm{erfc}\{\eta^{\frac{1}{2}}|\mathbf{r}_l - \mathbf{r}|\} \qquad (9)$$

where erf is the error function and erfc is the complimentary error function. Equation 9 reduces to Equation 5 when r goes to zero. When r is at the location of another ion, the potential is infinite.

An important immediate use we found for this perturbed form of the Ewald method was in calculating the potential at the sites of the oxygen atom vacancies between the Cu-O "chains" of the superconductor. Above approximately 700C, when the superconductor is in the tetragonal phase, there is roughly a 50% probability than any chain or interchain site will be occupied by an oxygen atom; while in the orthorhombic phase, there is nearly a 100% probability of occupancy of the chain sites only.[1]. We found an electrostatic potential at the site of the vacancy in the orthorhombic phase of -0.14Å^{-1}, indicating that a negative oxygen ion would not occupy this site. This negative potential in the orthorhombic phase indicates that the ortho-

LATTICE CONSTANTS: a = 3.8231 Å, b = 3.8864 Å, c = 11.6807 Å

ATOM	x/a	y/b	z/c	CHARGE	ELECTROSTATIC POTENTIAL ($Å^{-1}$)
Y	1/2	1/2	1/2	3.0	-1.74
Ba	1/2	1/2	0.1843	2.0	-1.41
Cu1	0	0	0	2.0	-2.18
Cu2	0	0	0.3556	2.5	-1.89
O1	0	1/2	0	-2.0	1.04
O2	1/2	0	0.3773	-2.0	1.84
O3	0	1/2	0.3789	-2.0	1.83
O4	0	0	0.1584	-2.0	1.22

Table 2

Lattice Parameters and the electrostatic potential at lattice sites for the superconductor $YBa_2Cu_3O_7$.

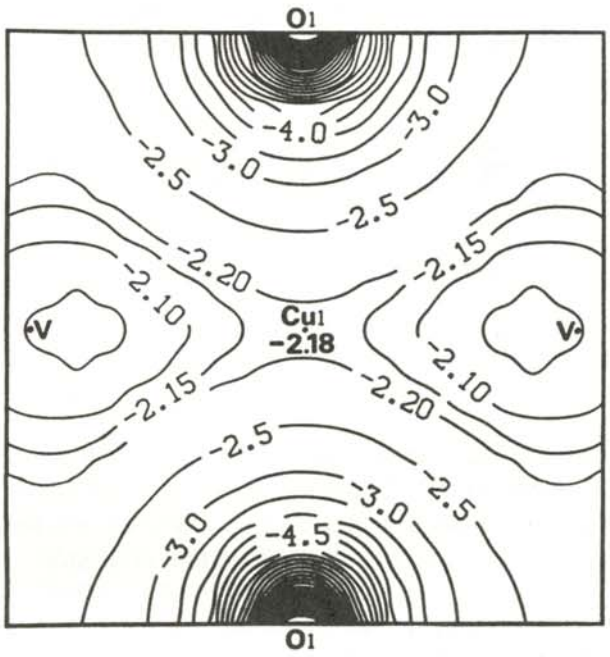

Figure 4
Contour plot of the electrostatic potential ($Å^{-1}$) in the plane of the Cu-O "chains" of the high T_c superconductor $YBa_2Cu_3O_7$ centered around the Cu1 site. The potential is computed in the absence of the copper (2+) ion. The copper, oxygen and vacancy sites are labeled Cu1, O1 and V respectively. Note that the electrostatic potential contours are more closely spaced below -2.5 $Å^{-1}$.

rhombic/tetragonal phase transition and the oxygen partial pressure surrounding the material are connected.

We then computed the potentials at a series of points within the crystal to produce a contour plot (typically at 50 locations within an area of $2Å^2$) showing the lines of electrostatic equipotential within the ionic crystals. The contour plots, Figures 4 and 5, produced using the DISSPLA graphics software available at Oak Ridge National Laboratory, show the electrostatic potenials of $YBa_2Cu_3O_7$ in the plane containing the Cu-O "chains". Figure 4 shows the potential in the absence of the copper 2^+ ion. Figure 5 shows the potential in the presence of the CuO chains. Note that the potential at the Cu1 site is -2.18 $Å^{-1}$ and at the vacancy site is - 0.14$Å^{-1}$ as predicted by Equation 5.

The contour plots show that the locations of the ions are relative potential maxima, indicating that these would not be points of stable equilibrium for the ions. This results because we assumed that the potentials were only ionic and did not take into consideration short range repulsive potentials. The lattice energies of these extra terms, although much smaller than the Madelung term, would be required to properly reproduce the conditions for stability of the experimentally observed structure of the high T_c superconductor.

SUMMARY

We presented the calculation of the Madelung constant for the high-T_c superconductor $YBa_2Cu_3O_7$ assuming that the binding of the atoms is predominantly ionic. We demonstrated the validity of the calculation by obtaining results for known ionic structures: NaCl, CuO, Cu_2O, BaO and Y_2O_3. We also obtained, using a perturbed form of the Ewald formula for the electrostatic potential at a lattice site, a contour plot for the electrostatic potential in the plane of the Cu-O "chains". We demonstrated that the potential at the oxygen vacancy site in the superconducting state would give a repulsive force to the introduction of an oxygen ion. Finally, we show that the Ewald method for computing the Madelung energy provides a useful tool for examining the electrostatic potential energy within a lattice.

ACKNOWLEDGMENTS

The author would like to thank Dr. William Butler and Dr. Nancy Wright at Oak Ridge National Laboratory for their valuable help in this work. He also acknowledges his advisor, Dr. Richard Ward, for the guidance and kindness shown him during his stay at Oak Ridge National Laboratory.

REFERENCES

* This work was supported by a Student Research Fellowship from Oak Ridge Associated Universities.

a) Present address: Physics Department, University of Massachusetts, Amherst, Amherst, MA 01003.

1) M.A. Beno, L. Soderholm, D.W. Capone II, D.G. Hinks, J.D. Jorgensen, J.D. Grace and I.K. Schuller, Appl. Phys. Lett., 51, 1987, p. 57.

2) P.P. Ewald, Ann. der Phys., 64, 1921, p. 253.

3) C. Kittel, Introduction to Solid Sate Physics 2nd Ed., John Wiley, New York, 1956, pp. 571-574.

4) L.C. Pauling, The Nature of the Chemical Bond 3rd Ed., The Cornell University Press, Ithaca, NY, 1960, p. 507.

5) M.J.L. Sangster and M. Dixon, Advances in Physics, 25, 1976, p. 247.

6) H.M. Evjen, Phys. Rev., 39, 1932, p. 675.

7) R.W.G. Wyckoff, Crystal Structures, 2nd Ed. Volume 1, John Wiley, New York, 1963.

8) R.W.G. Wyckoff, Crystal Structures, Volume 2, John Wiley, New York, 1964.

FACULTY SPONSOR

Dr. Richard Ward
Computing and Telecommunications Division
of Martin Marietta Energy Systems, Inc.
Oak Ridge National Laboratory
PO Box 2008, MS 6243 4500N
Oak Ridge, TN 37831

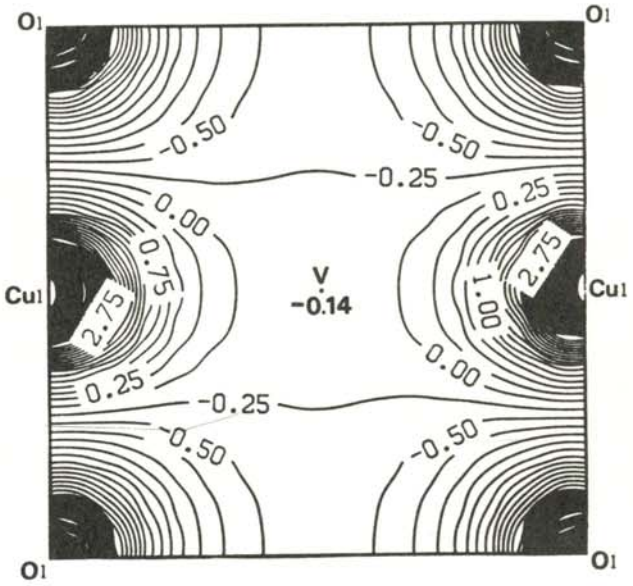

Figure 5
Contour plot of the electrostatic potential ($Å^{-1}$) in the plane of the Cu-O "chains" of the high-T_c superconductor $YBa_2Cu_3O_7$ centered around the vacancy site. The potential is computed in the presence of the CuO chain. The copper, oxygen and vacancy sites are labeled Cu1, O1 and V respectively.

MEASUREMENT OF COAGULATION PROCESSES BY LIGHT SCATTERING TECHNIQUES

Lee Fraiji
Department of Physics
Union College
Schenectady, NY 12308

ABSTRACT

Coagulation is a process whereby colloidal particles in water solutions are aggregated to form larger particles called flocculants. Because of their sizes, the flocculants begin to settle at the bottom of the solution and are easily removed by filtration. This project investigates a method for monitoring the entire coagulation process by laser light scattering.

INTRODUCTION

The large scale purification of drinking water is an important process in water treatment plants. Coagulation, followed by filtration, is the method of choice for separating solids from turbid water. While this technique can be traced back to the beginnings of recorded history, it was not employed in municipal water treatment until 1884 when Isaiah Hyatt patented a process of coagulation followed by rapid filtration. [1]

When a polymer, such as polyaluminum sulfate is added to waste water, coagulation begins to occur. Adding the polymer to waste water is an essential part of the solid-liquid separation procedure employed by many of the municipal water treatment plants throughout the United States. The coagulation process can be monitored by light scattering techniques. One such technique involves focusing a narrow beam of laser light on solutions contained in thin cells.[2] We, however, have concentrated our efforts on monitoring the process by passing a wider laser beam through larger volumes of solution.

We chose to use a wide beam laser for several reasons. The scattering of a wide beam is less dependent on individual particles and, therefore, produces a measurement which is an accurate representation of the amount of an 'average' size particle in the solution rather than the size of the individual particles. Also, wider beam lasers are generally more economical because they operate at low power and don't contain the sophisticated and costly optical components necessary to generate a narrow beam.

To appreciate the significance of such a project, one should understand some of the theory behind the formation of coagulants. The electrical double

---

Lee is a junior liberal arts-science major. He is a member of the college swim team. He intends to go to graduate school, probably in chemistry.

layer model [3] provides a good representation of the physical mechanisms which control the coagulation process. When a colloidal particle is immersed in water, charges develop on its surface. These charges are the result of the dissociation of ionizable groups on the colloid surface or the adsorption of low molecular weight ions onto the same surface. To maintain an electrically neutral solution, the charges in the vicinity of the colloid surface must be balanced by ions in the solution.

When a polymer is added to a solution containing colloids, at first it is perfectly soluble. If the polymer contains charged sites along its chain, the colloids will migrate to these charges to form a large electrically neutral insoluble particle called a flocculant. This resulting flocculant is too large to remain suspended in the solution and eventually sinks to the bottom. The latter process is called sedimentation. This project is primarily concerned with the kinetics of the flocculant formation.

There are two factors which determine the rate of flocculation. The first is the rate at which the polymer is dissolved and adsorbed onto the surface of the colloid. This rate is strongly dependent on the concentration of the polymer. The second is the rate at which the colloidal particles mesh together to form a large aggregate of particles. This rate can be related to the amount of kinetic energy imparted to the solution by each particle. If the particles move too quickly, their kinetic energies are high enough to overcome the potential energy generated by the attractive electrostatic forces between particles, and an aggregate will not form.

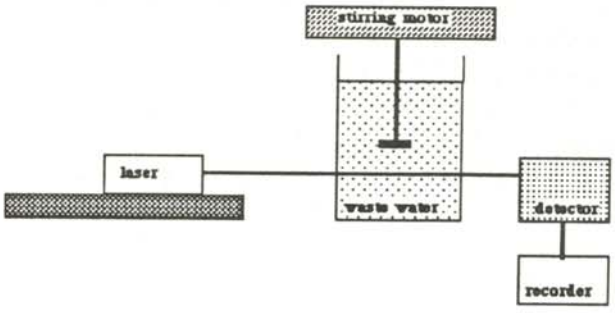

Figure 1
Experimental apparatus used to monitor the coagulation process by scattering of laser light.

The rate of the second step is limited by the first step. Since each flocculant is formed by the merger of several polymers, it is the concentration of the polymer that ultimately determines the degree of flocculation. Thus, the amount of flocculants formed will never exceed the amount of polymer added. Yet, if the polymer concentration is too high, the suspension becomes so crowed that the flocculants are not able to grow into large enough aggregates to form a sediment.

The rate of the second step is also determined by the amount of mixing in the solution. While mixing may enhance the first step by increasing the probability of a collision between a polymer and a colloid, it deters the aggregation of flocculants by imparting a large kinetic energy to them. To maximize the rate of the entire process, an polymer concentration which is not high enough to induce crowding and not low enough to reduce the rate of the first step must be attained. In addition, mixing must be terminated at the end of the first step. The second step is the slow step. Anything that can be done to increase the rate of this step will shorten the overall process

EXPERIMENTAL APPARATUS

Figure 1 is a schematic representation of the apparatus used to monitor the coagulation of waste water. Solutions of water water in a 1 liter plexiglass cell were placed underneath an electric stirring motor. A flat stainless steel stirring spoon extended from the motor into the cell. One one side of the cell was a low power (0.5 mW) He/Ne laser which was directed through the cell to a photodiode detector placed on the opposite side of the cell. The photodiode signal was amplified and interfaced to a meter and chart recorder. The detector could detect from 0 to 300 lux.

The polyaluminum sulfate was added by pipette to the cell containing constant pH waste water solutions while solution was being mechanically mixed. As coagulants began to form, the amount of transmitted light was recorded as a function of time.

A cell containing deionized water was used as a reference. The absolute signals of the two cells

were compared because the method only employed the use of a single laser beam.

RESULTS AND DISCUSSION

Our results show that the entire coagulation process can be measured by light scattering techniques in which the intensity of the laser beam passing through the solution was plotted as a function of time. The data, shown in Figure 2, showed that upon the addition of polyaluminum sulfate, a sharp decline in intensity was detected. This decline was short lived and was followed by a second decline which was longer and less steep.

The first decline was caused by the scattering of light due to the formation of coagulants (polymer-colloid complexes), This is the first step of the proposed mechanism. The second decline corresponded to the second step of the mechanism. It resulted from the formation of flocculants which are larger aggregated particles which scatter more light. Because the second decline was less steep than the first, it can be deduced that the second step was the slower step of the mechanism.

The signal steadily decreased until the maximum flocculant concentration occured. During sedimentation, the signal began to increase slowly. Ultimately, the signal rose above the level of the untreated waste water, but would never rise above the pure water reference.

When 5 ml of the polyaluminum sulfate solution was added to a solution of waste water, the signal decreased by 8 mV in 4.5 seconds and then decreased another 7 mV in 114 seconds. The maximum flocculant concentration occurred 4.5 minutes after the addition of the polyelectrolyte and brought about a 16mV decrease in the signal relative to the untreated waste water solution. Sedimentation was completed 2.5 hours later and was characterized by a signal which was 5 mV higher than the initial untreated sample, but was still 4 mV lower than that of the deionized water reference.

It is important to note that the signal produced by our methods was not a steady DC signal. Instead, the signal seemed to fluctuate over a range about an average. Thus, when we speak of an increase or decease in the signal, it is to this average which we refer, However, there is much to be learned from these fluctuations.

When the polymer is first added, most of the particles are of a uniform size and are moving at the same rate because the solution is being mixed. Thus, the signal fluctuates over a constant range and at a slightly higher frequency that it would during sedimentation. During this phase of the process, the signal fluctuates over a large range at lower frequencies because the flocculants encompass a wide range of sizes and move at slower rates because the solution is still. The rate at which the particles move through the beam determines the signal frequency and the relative continuity of particle size determines the range over which the signal fluctuates.

Our results seem to indicate that laser scattering is a simple and efficient method for monitoring the coagulation process. The use of such a technique enables one to optimize the amount of flocculating agent needed to purify a sample of waste water and thereby eliminate the unnecessary expenses generated from adding the flocculating agent in excess.

ACKNOWLEDGMENTS

The author would like to thank Dr. Sandor Feher for his unending support and many helpful suggestions offered throughout the project. He would also like to thank Dr. Laszlo Baksay for his guid-

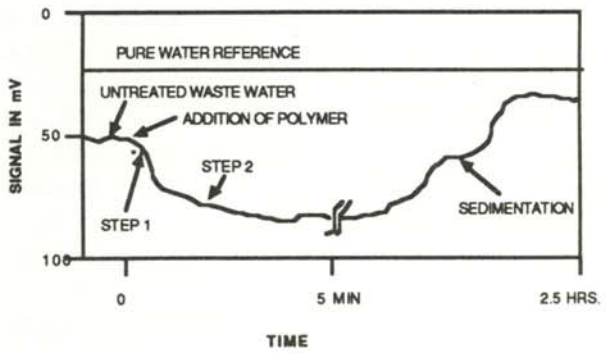

Figure 2
Typical response curve generated as coagulants scatter the laser beam during flocculation and sedimentation.

ance and encouragement. Finally, the author gratefully acknowledges the financial support of the Benzsay and Harrison Company of Delanson, NY which made this project possible.

REFERENCES

1) J.E. Singley, et.al. "State of the Art of Coagulation", Journal of the American Waterworks Association, 63,2, 1971.

2) J. Gregory and D.W. Nelson, "A New Optical Method for Flocculation Monitoring", Solid Liquid Separation, Ellis Holwood, Chichester, 1984.

FACULTY SPONSOR

Dr. Laszlo Baksay
Physics Department
Department of Physics
Union College
Science and Engineering Center
Schenectady, NY 12308-2311

Post Use Book Review

PHYSICS FOR SCIENTISTS AND ENGINEERS, 2ND. ED.

Raymond A. Serway, Saunders College Publishing, 1986

Reviewed by:

Jodi L. Barnhill
University of Arizona
Tucson, AZ 85721

In light of the current lack of physicists in the United States, the existence of a good physics book for introductory courses is more important than ever. Let us consider what criteria a beginning text should meet and whether **Physics for Scientists and Engineers** meets these criteria.

The physics text should be easily understandable and contain many interesting and useful analogies for the physical laws and ideas presented. While Serway's book is understandable, it falls far short of providing enlightening physical analogies. Perhaps the text contains too much quantitative information and not enough qualitative discussion. An example of this is the discussion of the law of universal gravitation. Serway states the law, gives the value for the gravitational constant, but does not give any analogies. In contrast, in the **Feynman Lectures on Physics**, when Richard Feynman discusses the same law, he notes:" In those days, one of the theories proposed was that the planets went around because behind them were invisible angles, beating their wings and driving the planets forward. ... It turns out that in order to keep the planets going around, the invisible angles must fly in a different direction and they have no wings. Otherwise, it is a somewhat similar theory!" He then remarks "If there is a force towards the sun, then the sun might be the angle, of course!"[1] What a delightful and refreshing way to introduce universal gravitation. I am not suggesting that all physics students must be entertained to grasp physics, but there are two ways to write a physics text: one can make it very formal and hum-drum or one can make it exciting and interesting. The latter method will probably create a more effective book.

Besides being understandable and giving good analogies, the text should enlighten the student about how and why major laws and theories were developed by giving historical information as well as the thinking behind why old theories got thrown out and how new ones got developed. Most texts available do not come close to meeting this criterion, and Serway is no exception. Since most physics texts are oriented towards engineering majors, they do not include historical and cultural points of view. Perhaps a problem solving text should be used in conjunction with a separate text, such as Feynman's book, that presents historical and cultural insight for physics majors as well as teaching them the foundations of physics. In this manner, the student leans how new theories were developed and also understand the significance of the theories.

Most importantly, the text should contain a plethora of problems for beginning, intermediate and ad-

---

Jodi is a senior physics major at the University of Arizona where she is a research assistant at the Lunar and Planetary Lab, President of the Soceity of Physics Students and an active member of the University Honors Program. She plans on specializing in optics and atmospheric sciences in graduate school.

vanced problem solvers. Answers for at least half of the problems should be included. These problems should prepare the undergraduate for upper division course work and the Graduate Record Examinations. While Serway does have problems for all skill levels, the answers to too many problems are incorrect. Some of the problems even have conceptual errors. When some of the professors at the University of Arizona explained to the editors that the book had numerous errors and explicitly pointed out the errors, they sent many students and professor new books that were supposed to be corrected. However, our new books had just as many errors as before. If honest corrections have been made to Serway's book since the edition that I am reviewing, it might be worth looking at the problems. Otherwise, one should not consider using this book.

I do not believe that Serway is the best choice for an undergraduate introductory physics text because it is not interesting enough and it contains too many errors in the problems. For the forty-five dollars that the text costs, a student could probably purchase Halliday and Resnick's book [2] which contains a very good set of problems and answers or two volumes of the **Feynman Lectures in Physics**. These books will be very worth while for the student, both as beginning texts and as reference books. The chances are better that the student will not be as hostile after using these books as after using Serway's book. It would be in a professor's as well as the student's best interest to choose these texts over **Physics for Scientists and Engineers**.

1) R.P. Feynman, R.B. Leighton and M.Sands, Feynman Lectures on Physics, Addison-Wesley, Reading MA, 1963.

2) B. Halliday and R. Resnick, Fundamentals of Physics, 3rd Ed., Wiley, New York, 1988.

The Journal of Undergraduate Research in Physics

The *Journal of Undergraduate Research in Physics* is the journal of Sigma Pi Sigma and the Society of Physics Students. It is published by the Physics Department of Guilford College, Greensboro NC. Inquiries about the journal should be sent to the editorial office.